1 **PM$_{2.5}$ concentrations based on near-surface visibility in the Northern Hemisphere from**
2 **1959 to 2022**

3 Hongfei Hao[1], Kaicun Wang[2], Guocan Wu[1], Jianbao Liu[2], Jing Li[3]

4 [1]Global Change and Earth System Science, Faculty of Geographical Science, Beijing Normal
5 University, Beijing 100875, China

6 [2]Institute of Carbon Neutrality, Sino French Institute of Earth System Science, College Urban and
7 Environmental Sciences, Peking University, Beijing 100871, China

8 [3]Institute of Carbon Neutrality, Sino French Institute of Earth System Science, Department of
9 Atmospheric and Oceanic Sciences, School of Physics, Peking University, Beijing 100871, China

10 Corresponding Author: *Kaicun Wang* Email: kcwang@pku.edu.cn

Abstract

12 Long-term PM$_{2.5}$ data are essential for the atmospheric environment, human health, and climate
13 change. PM$_{2.5}$ measurements are sparsely distributed and of short duration. In this study, daily PM$_{2.5}$
14 concentrations are estimated using a machine learning method from 1959 to 2022 in the Northern
15 Hemisphere based on near-surface atmospheric visibility, which are extracted from the Integrated
16 Surface Database (ISD). Daily continuous monitored PM$_{2.5}$ concentration is set as the target, and
17 near-surface atmospheric visibility and other related variables are used as the inputs. The 80% of
18 the samples of each site are the training set, and the 20% are the testing set. The training result
19 shows that the slope of linear regression with a 95% confidence interval (CI) between the estimated
20 PM$_{2.5}$ concentration and the monitored PM$_{2.5}$ concentration is 0.955 [0.955, 0.955], the coefficient
21 of determination (R^2) is 0.95, the root mean square error (RMSE) is 7.2 µg/m^3, and the mean
22 absolute error (MAE) is 3.2 µg/m^3. The test result shows that the slope within a 95% CI between
23 the predicted PM$_{2.5}$ concentration and the monitored PM$_{2.5}$ concentration is 0.864 [0.863, 0.865],
24 the R^2 is 0.79, the RMSE is 14.8 µg/m^3, and the MAE is 7.6 µg/m^3. Compared with a global PM$_{2.5}$
25 concentration dataset derived from satellite aerosol optical depth product with 1 km resolution, the
26 slopes of linear regression on the daily (monthly) scale are 0.817 (0.854) from 2000 to 2021, 0.758
27 (0.821) from 2000 to 2010, and 0.867 (0.879) from 2011 to 2022, indicating the accuracy of the
28 model and the consistency of the estimated PM$_{2.5}$ concentration on the temporal scale. The
29 interannual trends and spatial patterns of PM$_{2.5}$ concentration on the regional scale from 1959 to
30 2022 are analyzed by Generalized Additive Mixed Model (GAMM), suitable for the situation with
31 an uneven spatial distribution of monitoring sites. The trend is the slope of the Sen-Theil estimator.
32 In Canada, the trend is -0.10 µg/m^3/decade and the PM$_{2.5}$ concentration exhibits an east-high to
33 west-low pattern. In the United States, the trend is -0.40 µg/m^3/decade, and PM$_{2.5}$ concentration
34 decreases significantly after 1992, with a trend of -1.39 µg/m^3/decade. The high PM$_{2.5}$ concentration
35 areas are in the east and west and the low are in the central and northern regions. In Europe, the
36 trend is -1.55 µg/m^3/decade. High concentration areas are distributed in eastern Europe, and the low
37 areas are in northern and western Europe. In China, the trend is 2.09 µg/m^3/decade. High
38 concentration areas are distributed in northern China and the low areas are distributed in southern
39 China. The trend is 2.65 µg/m^3/decade up to 2011 and -22.23 µg/m^3/decade since 2012. In India, the
40 trend is 0.92 µg/m^3/decade. The concentration exhibits a north-high to south-low pattern, with high

41 concentration areas distributed in northern India, such as Ganges Plain and Thar Desert and the low
42 area is in Deccan Plateau. The trend is 1.41 μg/m^3/decade up to 2013 and -23.36 μg/m^3/decade since
43 2014. The variation in regional PM$_{2.5}$ concentrations is closely related to the implementation of air
44 quality laws and regulations. The daily site-scale PM$_{2.5}$ concentration dataset from 1959 to 2022 in
45 the Northern Hemisphere is available at National Tibetan Plateau / Third Pole Environment Data
46 Center (https://doi.org/10.11888/Atmos.tpdc.301127) (Hao et al., 2024).

Keywords

48 Fine particulate matter; PM$_{2.5}$; Visibility; Machine learning; Dataset.

1 Introduction

50 Fine particulate matter (PM$_{2.5}$) refers to particulate matter suspended in air with an aerodynamic
51 diameter of less than 2.5 micrometers. PM$_{2.5}$ has various shapes and is composed of complex
52 components, such as inorganic salts (e.g., sulfate, nitrate, and ammonium), as well as organic carbon
53 and elemental carbon, metallic elements, and organic compounds (Chen et al., 2020; Fan et al.,
54 2021). PM$_{2.5}$ can be emitted directly into the atmosphere (Viana et al., 2008; Zhang et al., 2019) and
55 generated through photochemical reactions and transformations (Guo et al., 2014). PM$_{2.5}$ exhibits
56 high concentrations near emission sources, which gradually decreases with distance. Due to the
57 smaller size and longer life span compared with coarse particulate matter, PM$_{2.5}$ can be transported
58 over long distances by atmospheric movements, leading to wide-ranging impacts. Studies indicate
59 that regional transport contributes significantly to local PM$_{2.5}$ concentration (Wang et al., 2014;
60 Chen et al., 2020).

61 PM$_{2.5}$ reduces atmospheric visibility and facilitates the formation of fog and haze conditions (Fan
62 et al., 2021). Direct and indirect effects of PM$_{2.5}$ on solar radiation in the atmosphere (Albrecht,
63 1989; Ramanathan et al., 2001; Bergstrom et al., 2007; Chen et al., 2022) alter the energy balance
64 and the number of condensation nuclei, thereby influencing atmospheric circulation and the water
65 cycle (Wang et al., 2012; Liao et al., 2015; Samset et al., 2019; Li et al., 2022).

66 PM$_{2.5}$ is also known as respirable particulate matter. Due to its complex composition, PM$_{2.5}$ may
67 carry toxic substances that can significantly impair human health. The World Health Organization
68 states explicitly that PM$_{2.5}$ is more harmful than coarse particles, and long-term exposure to high
69 PM$_{2.5}$ concentrations increases the risk of respiratory diseases, cardiovascular diseases, and lung
70 cancer (Lelieveld et al., 2015), regardless of a country's development status. A Global Burden of
71 Diseases study reveals that exposure to environmental PM$_{2.5}$ causes thousands of deaths and
72 millions of lung diseases annually (Chafe et al., 2014; Kim et al., 2015; Cohen et al., 2017).

73 PM$_{2.5}$ is an important parameter for assessing particulate matter pollution and air quality (Wang et
74 al., 2012). PM$_{2.5}$ can lead to soil acidification, water pollution, disruption of plant respiration, and
75 ecological degradation (Wu and Zhang, 2018; Liu et al., 2019). Due to globalization and economic
76 integration, preventing and controlling particulate matter pollution is a challenge at city, country
77 and global scales.

78 Therefore, long-term PM$_{2.5}$ concentration data are needed for studies on the environment, human
79 health, and climate change. At present, ground-based measurements, chemical models, and
80 estimations of alternatives are the primary sources of PM$_{2.5}$ concentration data.

81 Ground-based measurements are the most effective means to measure $PM_{2.5}$ concentration. $PM_{2.5}$
82 monitoring has been ongoing since the 1990s in North America and Europe (Van Donkelaar et al.,
83 2010), and large-scale $PM_{2.5}$ monitoring has been implemented in other regions since 2000,
84 including China in 2013 (Liu et al., 2017). As a result, the records for $PM_{2.5}$ concentration are short,
85 with only a few years of data available in many countries. The scarcity of $PM_{2.5}$ measurements
86 makes it challenging to provide long-term historical data for research.

87 Many studies have employed statistical methods, machine learning and deep learning methods to
88 estimate $PM_{2.5}$ concentrations based on aerosol optical depth. Van Donkelaar et al. (2021) has
89 utilized satellite aerosol optical depth data, aerosol vertical structure of chemical transport models,
90 and ground-level measurements to estimate monthly $PM_{2.5}$ concentrations and their uncertainties
91 over global land from 1998 to 2019, and there are several related studies (Van Donkelaar et al., 2010;
92 Boys et al., 2014; Van Donkelaar et al., 2015; Van Donkelaar et al., 2016; Hammer et al., 2020).
93 Many studies have been conducted at the regional scale, such as in the United States (Beckerman et
94 al., 2013), China (Wei et al., 2019b; Xue et al., 2019; Wei et al., 2020; He et al., 2021; Wei et al.,
95 2021), and India (Mandal et al., 2020). Although the $PM_{2.5}$ concentrations derived from satellite
96 retrievals have high spatial coverage, there are some limitations that need to be considered. Aerosol
97 optical depth describes the column property of aerosol, while $PM_{2.5}$ concentration describes the
98 near-surface properties of aerosol. Therefore, aerosol vertical structure is crucial in establishing the
99 relationship between the two. The daily representativeness is also considerable, as $PM_{2.5}$
100 concentration is continuously monitored while the daily frequency of satellite observations is low
101 (1-2 times). Surface types, cloud conditions (Wei et al., 2019a) and resolution (Nagaraja Rao et al.,
102 1989; Hsu et al., 2017) affect the accuracy of satellite products, thereby increasing uncertainty of
103 estimation of $PM_{2.5}$ concentration.

104 Reanalysis datasets provide estimates of long-term particulate matter concentrations. The Modern-
105 Era Retrospective Analysis for Research and Applications version 2 (MERRA-2) is an excellent
106 reanalysis dataset from NASA that uses the Goddard Earth Observing System version 5 (GEOS-5),
107 which provides global $PM_{2.5}$ data since 1980 (Buchard et al., 2015; Buchard et al., 2016; Buchard
108 et al., 2017; Gelaro et al., 2017; Sun et al., 2019). There are some emission inventories in the aerosol
109 model, including: volcanic material; monthly biomass burning from 1980 to 1996; monthly SO_2,
110 SO_4, POM, and BC from 1997 to 2009; annual anthropogenic SO_2 between 100 and 500 m above
111 the surface from 1980 to 2008; annual anthropogenic SO_4, BC, and POM concentrations from 1980
112 to 2006. In assimilation systems, satellite aerosol products from MISR and MODIS Aqua/Terra are
113 assimilated after 2000. Another reanalysis dataset is the Copernicus Atmosphere Monitoring Service
114 (CAMS) global reanalysis, which is a global reanalysis dataset of the atmospheric composition
115 produced by the European Centre for Medium-Range Weather Forecasts (ECMWF) and has
116 provided $PM_{2.5}$ data since 2003 (Che et al., 2014; Inness et al., 2019). Although reanalysis provides
117 long-term $PM_{2.5}$ data, the uncertainty in emission inventories increases the uncertainty in $PM_{2.5}$
118 concentration (Granier et al., 2011). The validation of the reanalysis based on emission inventories
119 shows that $PM_{2.5}$ concentration is still overestimated or underestimated in some regions (Buchard
120 et al., 2017; Ali et al., 2022; Jin et al., 2022). The assimilation of aerosol optical depth products
121 improves the aerosol column properties (Buchard et al., 2017), thereby improving the estimation of
122 surface $PM_{2.5}$ concentration, as it to some extent constrains the vertical structure of aerosols.
123 However, the lack of high spatiotemporal resolution emission inventories and long-term

124   assimilation data greatly limits the accuracy of surface $PM_{2.5}$ concentrations.

125   Another alternative for estimating $PM_{2.5}$ concentrations is the near-surface atmospheric horizontal
126   visibility, which is the maximum distance at which observers with normal visual acuity can discern
127   target contours under current weather conditions. In addition to manual observations, automated
128   visibility measurement has been implemented early, typically relying on the aerosol scattering
129   principle (Wang et al., 2009; Zhang et al., 2020). Both visibility and $PM_{2.5}$ concentration are
130   measurements of near-surface aerosols. They describe atmospheric horizontal transparency and are
131   used to describe atmospheric pollution. Long-term visibility records have been used to quantify
132   long-term aerosol properties (Molnár et al., 2008; Wang et al., 2009; Zhang et al., 2017; Zhang et
133   al., 2020). Visibility observation stations are densely distributed across the world. Compared to
134   satellite retrievals, visibility observations have longer historical records dating back to the early 20th
135   century (Noaa et al., 1998; Boers et al., 2015), are not affected by cloud interference and provide
136   continuous measurements.

137   Visibility has been used as a proxy for $PM_{2.5}$ concentration (Huang et al., 2009) and to estimate
138    $PM_{2.5}$ concentration (Liu et al., 2017; Li et al., 2020; Singh et al., 2020). Singh et al. (2020) has
139   analyzed the air quality in East Africa from 1974 to 2018 using visibility data. Liu et al. (2017) has
140   developed a statistical model and utilized ground-level visibility data to estimate long-term $PM_{2.5}$
141   concentrations in China from 1957 to 1964 and 1973 to 2014. Gui et al. (2020) has proposed a
142   method to establish a virtual ground observation network for $PM_{2.5}$ concentration in China using
143   extreme gradient boosting modeling in 2018. Zeng et al. (2021) has used LightGBM to establish a
144   virtual network for hourly $PM_{2.5}$ concentrations in China in 2017. Zhong et al. (2021; 2022) has
145   used LightGBM to predict 6-hour $PM_{2.5}$ concentrations based on visibility, temperature, and relative
146   humidity in China from 1960 to 2020. Meng et al. (2018) has utilized a random forest model to
147   estimate the daily $PM_{2.5}$ components in the United States from 2005 to 2015. These studies have
148   provided various methods for estimating $PM_{2.5}$ using visibility data. However, some have focused
149   on only methodological innovations without providing long-term trends in $PM_{2.5}$ concentration.
150   Other studies offer long-term trends, but the primary focus is at urban ore national scale. There are
151   few studies on long-term and high-temporal-resolution $PM_{2.5}$ concentration at the global scale or
152   across different countries.

153   This study uses a convenient, accurate, and easily understandable machine learning approach to
154   estimate daily $PM_{2.5}$ concentrations based on visibility at 5023 land-based sites from 1959 to 2022.
155   First, we build a machine learning model and then analyze the importance of the variables. Second,
156   we evaluate the model's performance and predictive ability. Third, we discuss the errors and
157   limitations of the dataset. Fourth, we compare the estimated $PM_{2.5}$ concentration with the other
158   dataset. Finally, we analyze the long-term trends and spatial patterns of $PM_{2.5}$ concentration in
159   different regions. We hope the $PM_{2.5}$ dataset will provide support for the atmospheric environment,
160   human health, and climate change studies.

161   **2 Data and methods**

162   **2.1 Study Area**

163   The study area is the Northern Hemisphere. Figure 1 shows the distributions of visibility stations (a)
164   and the $PM_{2.5}$ monitoring sites (b). Table 1 lists information of stations such as the number and time

span in each region. The number of visibility stations and PM$_{2.5}$ monitoring sites is 5023. Due to its relevance to national or regional development, the record length and distribution of PM$_{2.5}$ observation are uneven. In this study, the site-scale PM$_{2.5}$ observations are met at least three years. These sites are densely populated in North America, East and South Asia, and Europe, and are very sparse in regions such as Africa and South America, and West Asia.
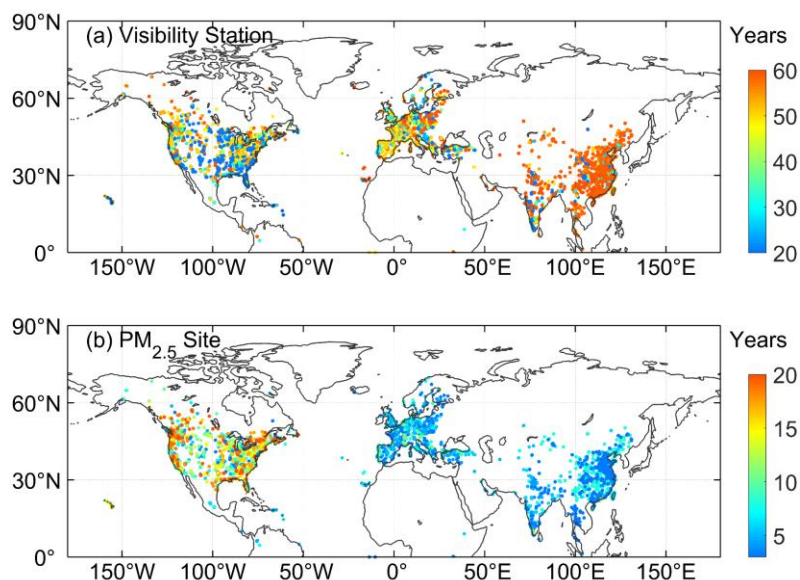
Figure 1. Study area and distributions of visibility stations (a) and PM$_{2.5}$ monitoring sites (b). The color of marker (circle) represents the year number of visibility observations and PM$_{2.5}$ concentration observations.

Table 1. Data summary.

	Region	Sites Number	Time Span	Temporal/Spatial Resolution	Data Source
Visibility	Global land	5023	1959-2022	Hourly/-	https://www.weather.gov/asos
	the United States	1111	1998-2022	Hourly/-	https://www.epa.gov/aqs
	Canada	311	1995-2022	Hourly/-	https://www.canada.ca
PM$_{2.5}$	Europe	1073	1998-2022	Hourly/-	https://european-union.europa.eu;https://www.eea.europa.eu
observations	China	1887	2014-2022	Hourly/-	https://www.cnemc.cn
	India	270	2010-2022	Hourly/-	https://app.cpcbccr.com
	Other regions	371	2016-2022	Hourly/-	https://openaq.org
LGHAP	Land (-58~62°N)	--	2000-2021	Daily/1km	https://zenodo.org/communities/ecnu_lghap

2.2 PM$_{2.5}$ Data

2.2.1 PM$_{2.5}$ Data in the United States

The hourly PM$_{2.5}$ concentration data for the United States from 1998 to 2022 are sourced from the Air Data System (AQS), which are available at https://www.epa.gov/aqs. The AQS provides PM$_{2.5}$ mass monitoring and routine chemical speciation data and contains other ambient air pollution data collected by the Environmental Protection Agency (EPA), state, local, and tribal air pollution control agencies from thousands of monitors, comprising the Federal Reference Method (FRM) and Federal

Equivalent Method (FEM). The primary purpose of both methods is to assess compliance with the $PM_{2.5}$ National Ambient Air Quality Standards (NAAQS). FRMs include in-stack particulate filtration, and FEMs include beta-attenuation monitoring, very sharp cut cyclones, and tapered element oscillating microbalances (TOEMs). The measurement precision is $\pm$ (1~2) $\mu g/m^3$ (hour) (Hall and Gilliam, 2016). The TEOM and beta-attenuation are automatic and near real-time monitoring methods. The TEOM, which is based on gravity, measures the mass of particles collected on filters by monitoring the frequency changes in tapered elements. The beta-attenuation method uses beta-ray attenuation and particle mass to measure the $PM_{2.5}$ concentration. In this study, we use two $PM_{2.5}$ measurement methods, FRM/FEM (88101) and non-FRM/FEM (88502). The 88502 monitors are "FRM-like" but are not used for regulatory purposes. Both the 88101 and 88502 monitors are used for reporting daily Air Quality Index values.

2.2.2 $PM_{2.5}$ Data in Canada

The hourly $PM_{2.5}$ concentration data for Canada from 1995 to 2022 are sourced from the National Air Pollution Surveillance (NAPS) program, which are available at https://www.canada.ca. The NAPS program is a collaborative effort between the Environment and Climate Change Canada and provincial, territorial, and regional governments and is the primary source of environmental air quality data. Since 1984, $PM_{2.5}$ concentrations have been measured in Canada using a dichotomous sampler. Continuous or real-time particle monitoring began in the NAPS network in 1995 using TEOM and beta-attenuation monitoring (Demerjian, 2000). The samples are supplemented by EPA FRM samples obtained after 2009 (Dabek-Zlotorzynska et al., 2011).

2.2.3 $PM_{2.5}$ Data in Europe

The hourly $PM_{2.5}$ concentration data for Europe from 1998 to 2012 are obtained from the AirBase database, which is available at https://european-union.europa.eu. The hourly $PM_{2.5}$ concentration data (E1a) from 2013 to 2022 are obtained from the AirQuality database, which is available at https://www.eea.europa.eu. AirBase is maintained by the European Environment Agency (EEA) through its European Topic Center on Air Pollution and Climate Change Mitigation. Airbase contains air quality monitoring data and information submitted by participating countries throughout Europe. After the Air Quality Directive 2008/50/EC was enforced, the $PM_{2.5}$ concentration data began to be stored in AirQuality database. The main monitoring methods for $PM_{2.5}$ concentration include TEOM and beta attenuation (Green and Fuller, 2006; Chow et al., 2008). The sites are distributed across rural, rural-near city, rural-regional, rural-remote, suburban, and urban areas.

2.2.4 $PM_{2.5}$ Data in China

The hourly $PM_{2.5}$ concentration data for China from 2014 to 2022 are obtained from the China National Environmental Monitoring Center, which are available at https://www.cnemc.cn. The continuous monitoring of $PM_{2.5}$ nationwide began in 2013 and $PM_{2.5}$ concentration data are available to the public. (Su et al., 2022), and there are about 2000 air quality observation sites in 2022. $PM_{2.5}$ concentrations are measured using the TEOM and beta-attenuation method (Zhao et al., 2016b; Miao and Liu, 2019). According to the China Environmental Protection Standards, instrument maintenance, data transmission, data assurance and quality control ensure the reliability of $PM_{2.5}$ concentration measurements. The uncertainty in the $PM_{2.5}$ concentration is < 5 $\mu g/m^{-3}$ (Pui

223   et al., 2014).

2.2.5 PM$_{2.5}$ Data in India

225   The hourly PM$_{2.5}$ concentration data for India from 2010 to 2022 are obtained from the Central
226   Pollution Control Board (CPCB), which are available at https://app.cpcbccr.com. The Air
227   (Prevention and Control of Pollution) Act of 1981 is enacted by the Central Pollution Control Board
228   (CPCB) of the Ministry of Environment, Forest and Climate Change (MoEFCC). The National Air
229   Quality Monitoring Programme (NQAMP) is a key air quality monitoring programme employed by
230   the Government of India, which is managed by the CPCB in coordination with the State Pollution
231   Control Boards (SPCBs) and UT Pollution Control Committees (PCCs). A standard of 60 μg/m^3
232   PM$_{2.5}$ concentration over 24 hours is added in 2009. The methods used by the Indian National
233   Ambient Air Quality Standards (NAAQS) for PM$_{2.5}$ concentration and related component
234   measurements include the FRM and FEM (Pant et al., 2019). The measurement precision is ± (1-2)
235   μg/m^3 (hour).

2.2.6 PM$_{2.5}$ data in other regions

237   The hourly PM$_{2.5}$ concentration data of other regions from 2016 to 2022 are from openAQ
238   (https://openaq.org), which is a nonprofit organization providing air quality data. These air quality
239   data are collected from environmental protection departments and other departments over the world
240   without any processing, therefore they have good accuracy. The PM$_{2.5}$ concentrations almost are
241   measured by the TEOM and beta-attenuation method, and have been used for scientific research
242   (Jin et al., 2022; Tan et al., 2022).

2.3 Visibility and Meteorological Data

244   The hourly visibility and meteorological data are from the Integrated Surface Database (ISD) (Smith
245   et al., 2011), which is a global database consisted of hourly and synoptic surface observations and
246   archived at the NOAA's National Centers for Environmental Information (NCEI), available at
247   https://www.ncei.noaa.gov/products/land-based-station/integrated-surface-database. The ISD
248   database integrates data from more than 100 original data sources and incorporates data from over
249   35000 stations around the world and includes observations data dating back to 1901. The strict
250   quality control algorithms are used to ensure data quality by checking data format, extreme values
251   and limits, consistency between parameters, and continuity between observations. Detailed
252   information about the quality control are in http://www.ncei.noaa.gov/pub/data/inventories/ish-
253   qc.pdf. The best spatial coverage of stations is evident in North America, Europe, Australia, and
254   parts of Asia, and the coverage in the Northern Hemisphere is better than the Southern Hemisphere.

255   Visibility and meteorological records are filtered by the geophysical report type code. The codes of
256   FM-12 and FM-15 are selected. FM-12 code represents the report is from Surface Synoptic
257   Observations (SYNOP) report, which is a coding system developed by the World Meteorological
258   Organization (WMO) for reporting observation data from ground meteorological stations. FM-15
259   code represents the report is from Meteorological Terminal Aviation Routine Weather Report
260   (METAR), providing weather information at the airport and its surrounding areas. The format and
261   content of the METAR report are consistent globally and comply with WMO's international
262   meteorological observation and reporting standards. The frequency of SYNOP report is generally
263   every three or six hours, and the frequency of METAR report is usually once per hour.

In this study, visibility is an essential variable for PM$_{2.5}$ concentration. The reciprocal of visibility is directly proportional to the aerosol extinction coefficient, which is closely related to the PM$_{2.5}$ concentration (Wang et al., 2009; Wang et al., 2012). Considering that temperature, wind speed, humidity, and precipitation are factors that impact particle dispersion, particle growth, and secondary generation (Zhang et al., 2020), temperature, dew point temperature, wind speed, and precipitation are selected.

2.4 Data Preprocessing

When processing the visibility and meteorological variables, we use some screening conditions from previous studies (Husar et al., 2000; Wang et al., 2009; Li et al., 2016; Zhong et al., 2021). We remove the records with missing visibility, temperature, dew point temperature, wind speed and hourly precipitation greater than 0.1 mm. Relative humidity is calculated using the Goff-Gratch formula (Goff, 1957). When relative humidity is greater than 90%, the record is removed to reduce the influence of fog, even precipitation. In high latitude regions, the low visibility records caused by ice fog and snow are removed, when the temperature is less than -29 ℃ and the wind speed is greater than 16 km/h. Since PM$_{2.5}$ exhibits hygroscopic growth, dry visibility is calculated, when relative humidity is between 30% and 90% (Yang et al., 2021).

$$VISD = VIS/(0.26 + 0.4285 * log(100 - RH)) \tag{1}$$

where VIS is the visibility, RH is the relative humidity, and VISD is the dry visibility.

For a single visibility site, there should be at least 5 non-repetitive visibility values and at least three valid records per day. The upper limit of visibility is set to the 99% percentile of visibility (Li et al., 2016). The harmonic mean is used to calculate the daily VIS and VISD because it can better capture rapid weather changes and enhance daily representativeness (Noaa et al., 1998). The arithmetic mean is used for other variables.

The maximum hourly PM$_{2.5}$ concentration is set to 1000 μg/m^3. The daily PM$_{2.5}$ concentration needs at least 3 hourly records. We select the PM$_{2.5}$ monitoring sites with a condition of at least 3-year continuous monitoring. The distribution of PM$_{2.5}$ sites is shown in Figure 1, and the details are shown in Table 1.

The spatial matching between PM$_{2.5}$ site and visibility station adopts the nearest principle, and the upper limit of distance is set to 100 km. Through experiments that the upper limit of distance has little effect on model training and prediction, but when the upper limit is small, the number of site pairs significantly decreases, especially in Asia. Matched visibility stations are not be used again. To match more PM$_{2.5}$ monitoring sites, we construct a 'virtual' visibility station, whose variables are established by the average of variables of the two nearest visibility stations.

We merge daily PM$_{2.5}$ concentration and visibility and other meteorological variables. We have adopted two matching methods: (1) merge at the hourly scale first and then calculate the daily mean (2) and calculate the daily mean first and then match. The results of two methods have no impact on the training of the model, but there are differences in the predicted results. Since SNOPY's visibility is not continuously observed hourly, we select the second method to merge PM$_{2.5}$ concentration and visibility data on the daily scale to improve the daily representativeness of estimated PM$_{2.5}$ concentration.

2.5 PM$_{2.5}$ Data for Comparison

The long-term gap-free high-resolution air pollutants (LGHAP) dataset provides daily PM$_{2.5}$ concentrations from 2000 to 2021 over global land, with a 1 km grid resolution, which is available at https://zenodo.org/communities/ecnu_lghap. The PM$_{2.5}$ concentration is estimated using aerosol optical depth and other factors such as geographic location, land cover type, climate zone, and population density, based on a deep-learning approach, termed the scene-aware ensemble learning graph attention network. The correlation coefficient with ground-based measurements is 0.95 and the RMSE is 5.7 μg/m^3 (Bai et al., 2024). This dataset provides global PM$_{2.5}$ concentration with a high spatiotemporal resolution.

For most regions in the Northern Hemisphere, except for North America and Europe, the duration of continuous monitoring PM$_{2.5}$ concentration data is relatively short, making it difficult to evaluate historical PM$_{2.5}$ concentration. For example, PM$_{2.5}$ monitoring network in China was implemented from the end of 2012, resulting in the inability to verify the PM$_{2.5}$ concentrations before 2012. Therefore, we compare our data with the LGHAP PM$_{2.5}$ concentration to evaluate the predictive ability of the model and the consistency of our data on the temporal scale.

2.6 Decision Tree Regression

We employ decision tree regression (Teixeira, 2004) to estimate daily PM$_{2.5}$ concentrations. The key to decision tree regression is to find the optimal split variable and optimal split point. The optimal split point of the predictor is determined by the minimum mean squared error, which determines the optimal tree structure. Decision tree regression is a commonly used nonlinear machine learning method that partitions the feature space based on the mapping between feature attributes and response values, with each leaf node representing a specific output for each feature space region. It's ability to handle complex relationships with relatively few model parameters is advantageous, minimizing the risk of overfitting and enabling the prediction of continuous and categorical predictive variables.

The sample data includes predictor and response. The predictor is composed of 9 variables: the reciprocal of dry visibility (Vis_Dry_In), the reciprocal of visibility (Vis_In), temperature (Temp), dew point temperature (Td), temperature-dew point difference (Temp-Td), relative humidity (RH), wind speed (WS), wind numerical time (DateTime) and daily record number (DailyObsNum). Both visibility and meteorological variables are daily means. The response variable is the daily monitored PM$_{2.5}$ concentration.

For each site, we sort the sample data by time, with the first 80% being the training set and the last 20% being the test set. Due to the inconsistent sample length among different sites, this approach is friendly for sites with small sample sizes (such as only 3-year observations).We use10-fold cross-validation method (Browne, 2000) to train the model. The test set is used to evaluate the predictive ability of the model.

2.7 Evaluation Metrics

2.7.1 Statistical Metrics

We use the root mean squared error (RMSE), mean absolute error (MAE), and correlation coefficient (ρ) as evaluation metrics to evaluate the model's performance and predictive ability. The

344   formulas are given as follows:

345    $$MSE = \sqrt{\frac{1}{n}\sum_{i=1}^{n}(y_i - \hat{y}_i)^2}$$ (2)

346    $$MAE = \frac{1}{n}\sum_{i=1}^{n}|y_i - \hat{y}_i|$$ (3)

347    $$\rho = \frac{\sum_{i=1}^{n}(y_i-\bar{y})(\hat{y}_i-\bar{\hat{y}})}{sqrt(\sum_{i=1}^{n}(y_i-\bar{y})^2\sum_{i=1}^{n}(\hat{y}_i-\bar{\hat{y}})^2)}$$ (4)

348   where y_i and $\bar{y}$ are the predicted value and the average of the predicted values. $\hat{y}_i$ and $\bar{\hat{y}}$ are
349   the target and the average of the target. $i = 1,2,\ldots,n$. n is the length of sample.

2.7.2 Partial Dependence

351   The importance of predictor variables is assessed via partial dependence. Partial dependence
352   represents the relationship between the individual predictive variable and the predicted response
353   (Friedman, 2001). By marginalizing the other variables, the expected response of the predicted
354   variable is calculated. All the partial dependences of the predicted response on the subset of
355   predicted variables are calculated. The calculation process of the partial dependency method is
356   described as follows:

357   The dataset of the predictor is X, $X = [X^1, X^2, \ldots, X^n]$, and n represents the number of predictive
358   factors. The complement of subset X^s is X^c, where X^s is a single variable in X and X^c is all
359   other variables in X. The predicted response $f(x)$ depends on all variables in X, and it is expressed
360   as follows:

361    $$f(x) = f(X^s, X^c)$$ (5)

362   The partial dependence of the predicted response to X^s is expressed as follows:

363    $$f^s(X^s) = \int f(X^s, X^c)pC(X^c)dX^c$$ (6)

364   where $pC(X^c)$ is the marginal probability of X^c, that is, $pC(X^c) \approx \int f(X^s, X^c)dX^s$. Assuming
365   that the likelihood for each observation is equal, the dependence between X^s and X^c and the
366   interactions of X^s and X^c in response are not strong. The partial dependence is shown below:

367    $$f^s(X^s) \approx \frac{1}{N}\sum_{i=1}^{N}f(X^s, X_i^s)$$ (7)

368   where N is the number of observations and i represents the ith observation.

2.7.3 Generalized Additive Mixed Model

370   Generalized Additive Mixed Model (GAMM) originates from two independent yet complementary
371   statistical methods: Generalized Additive Model (GAM) and Mixed Effects Models. GAM is
372   introduced by Trevor Hastie and Robert Tibshirani in the 1980s (Hastie and Tibshirani, 1987). GAM
373   employs smooth functions (such as splines) to replace linear terms in traditional regression,
374   capturing nonlinear relationships between response and explanatory variables. The primary aim of
375   GAM is to enhance model flexibility, allowing the data to determine the form of the nonlinear
376   relationships rather than pre-specifying them. Mixed Effects Model includes both fixed and random

377 effects, enabling the analysis of hierarchical and correlated data (Verbeke and Lesaffre, 1996). Fixed
378 effects apply to the entire sample, whereas random effects account for variations within individuals
379 or groups, explaining data correlation and variability. GAMM represents the evolution of statistical
380 models from linear to nonlinear, from simple to complex, and from single effects to mixed effects.
381 GAMM has been widely applied in various fields such as ecology and climate, air pollution
382 becoming essential tools for studying complex nonlinear relationships and hierarchical data (Park
383 et al., 2013; Polansky and Robbins, 2013; Chang et al., 2017; Ravindra et al., 2019).

384 The relationship between $PM_{2.5}$ concentrations and time (e.g., months, seasons) is typically
385 nonlinear and exhibits seasonal variation. GAMM model uses smooth functions (such as splines) to
386 capture the nonlinear variations and model the periodic features with cyclical smooth functions.
387 Interannual variations in $PM_{2.5}$ concentrations can also be captured using smooth functions. Due to
388 the inherent autocorrelation in time series, GAMM model effectively handles the autocorrelation by
389 incorporating time-related smooth functions or random effects, thereby enhancing the model
390 accuracy. $PM_{2.5}$ concentrations from neighboring locations often exhibit spatial correlation. GAMM
391 model can address this spatial correlation by introducing spatially correlated smooth functions or
392 random effects. Therefore, it is also suitable for spatial variations, especially when the spatial
393 distribution of sites observations is uneven.

394 Based on the GAMM, the $PM_{2.5}$ concentration $y(i, t)$ at site i and time t can be expressed as:

395 $$y(i, t) = x\beta + f(\cdot) + b(i, t) + \varepsilon(i, t) \tag{8}$$

396 The following is an explanation of the expression and parameter settings.

397 *Linear terms* $x\beta$: x is the vector of explanatory variables, including site elevation and the overall
398 mean $PM_{2.5}$ concentration. β is a coefficient vector.

399 *Smooth terms* $f(\cdot)$ can be decomposed into three individual smooth terms: seasonal smooth term,
400 interannual smooth term, and spatial smooth term, as shown in equation (9).

401 $$f(\cdot) = f(month) + f(year) + f(\text{spatial}) \tag{9}$$

402 They are composed of linear combinations using spline basis functions. For seasonal smooth term,
403 it is a function of the month, smooth function is the penalized regression cyclic cubic splines
404 (assumed with periodic nature) (Wood et al., 2016) and the knot number is 12. For interannual
405 smooth term, it is a function of the year, smooth function is the penalized regression cubic splines
406 (Wood et al., 2016) and the knot number is 64. For spatial smooth term, it is a function for longitude
407 and latitude, smooth function is the gaussian process penalized regression splines (Kammann and
408 Wand, 2003) and the knot number is 80. In this study, they are used to describe the regional long-
409 term $PM_{2.5}$ concentration annual cycle, interannual trends and spatial distribution, respectively.

410 Station-specific effects term $b(i, t)$ is a random effect term to describe the differences between
411 observation sites, based on the assumption that observations are independent.

412 The residual noise term $\varepsilon(i, t)$ 1-order autoregressive term.

413 More explanations about GAMM model are detailed in the package mgcv of R. Some studies also
414 provide an introduction and selection of parameters (Polansky and Robbins, 2013; Chang et al.,
415 2017; Ravindra et al., 2019).

3. Results and Discussion

3.1 Evaluation of Variable Importance

We evaluate the contribution of each variable to the response by partial dependence. The variable with the highest partial dependence value is the most important variable in the model. Figure 2 (a) shows the proportion of the most important variables for all sites and Figure 2 (b) shows the ranking of the importance of all variables. Reciprocal of dry visibility is the most important variable at 65.8% of sites, and Reciprocal of visibility is the second most important variable at 14.9% of sites. The contribution of meteorological variables ranges from 2.1% to 6.6%. The time variable contributes 1.7%. The lowest contribution is daily number of visibility record at only 0.9%, because it is only a variable that describes the daily representativeness of visibility. It also indicates that daily visibility has high daily representativeness (under the conditions of at least three hourly records)

The $PM_{2.5}$ concentration level varies spatially, which are related to regional geographical environment, climate, and air quality laws and regulations. Therefore, we analyze the importance of variables in different regions, as shown in Figure 2 (c-h). The two most important variables are still reciprocal of dry visibility and reciprocal of visibility, with a proportion of 73.1% in the United States, 77.5% in Canada, 80.8% in Europe, 98.8% in China, and 60.2% in India. It indicates that $PM_{2.5}$ concentration is the most significantly correlated with visibility in China. The contribution of meteorological variables is significantly higher in the United States and India than in other regions. It indicates that meteorological conditions have a significant contribution to $PM_{2.5}$ concentration in these regions, which may be related to the formation mechanism and transport of particulate matter.

The above results indicate a strong correlation between the $PM_{2.5}$ concentration and visibility, as visibility can be considered an indicator of air quality without fog or precipitation. Meteorological factors play secondary roles, which influence the formation, dispersion and deposition of $PM_{2.5}$ (Gui et al., 2020; Zhong et al., 2022). Although the number of daily records and time have the most negligible impacts on the $PM_{2.5}$ concentration in the model, they have significant impacts on the cyclical changes and daily representativeness of $PM_{2.5}$ concentration (Wang et al., 2012; Zhang et al., 2020).

443
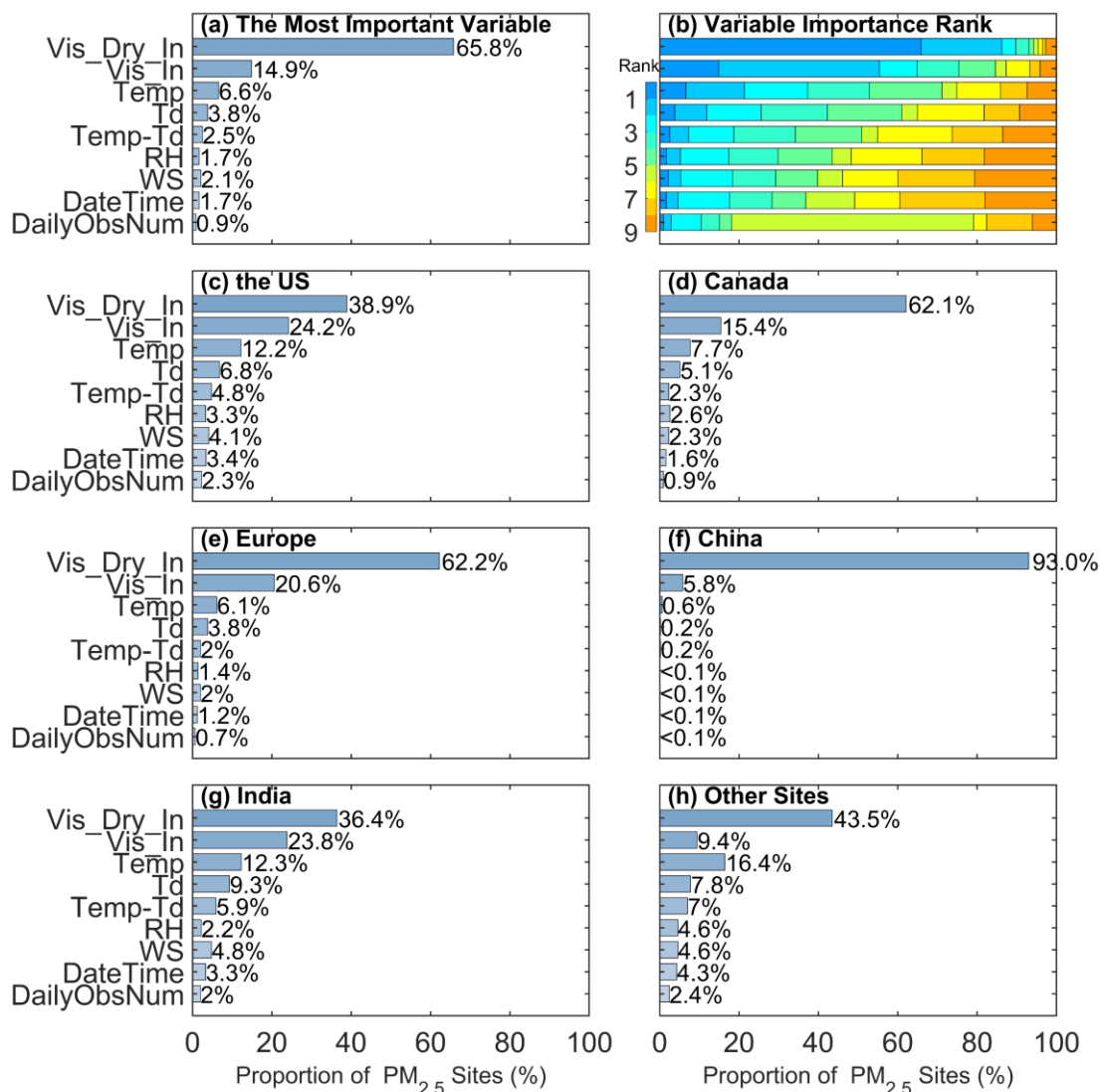
Figure 2. The most important variable (a) and the ranking (b) at all sites. The most important variable in each region (c-h). The stacked bar shows the importance rankings of the variables ('rank=1' represents the most important variable). The bar shows the proportion of the most important variable. The variables are the reciprocal of dry visibility (Vis_Dry_In), reciprocal of visibility (Vis_In), temperature (Temp), dew point temperature (Td), temperature-dew point difference (Temp-Td), relative humidity (RH), wind speed (WS), numerical time (DateTime) and daily number of visibility record (DailyObsNum).

3.2 Evaluation of Model Performance

We analyze the linear regression relationship between all estimated and corresponding response values to evaluate the model's performance. Figure 3 is the density scatter plot of the monitored $PM_{2.5}$ concentration (response values) and the estimated $PM_{2.5}$ concentration (estimated values). There is a total of 8031473 data pairs for all the sites. The linear regression slope (95% confidence interval) is 0.955 [0.955, 0.955], the R^2 is 0.95, the RMSE is 7.2 $\mu g/m^3$, and the MAE is 3.2 $\mu g/m^3$.

457
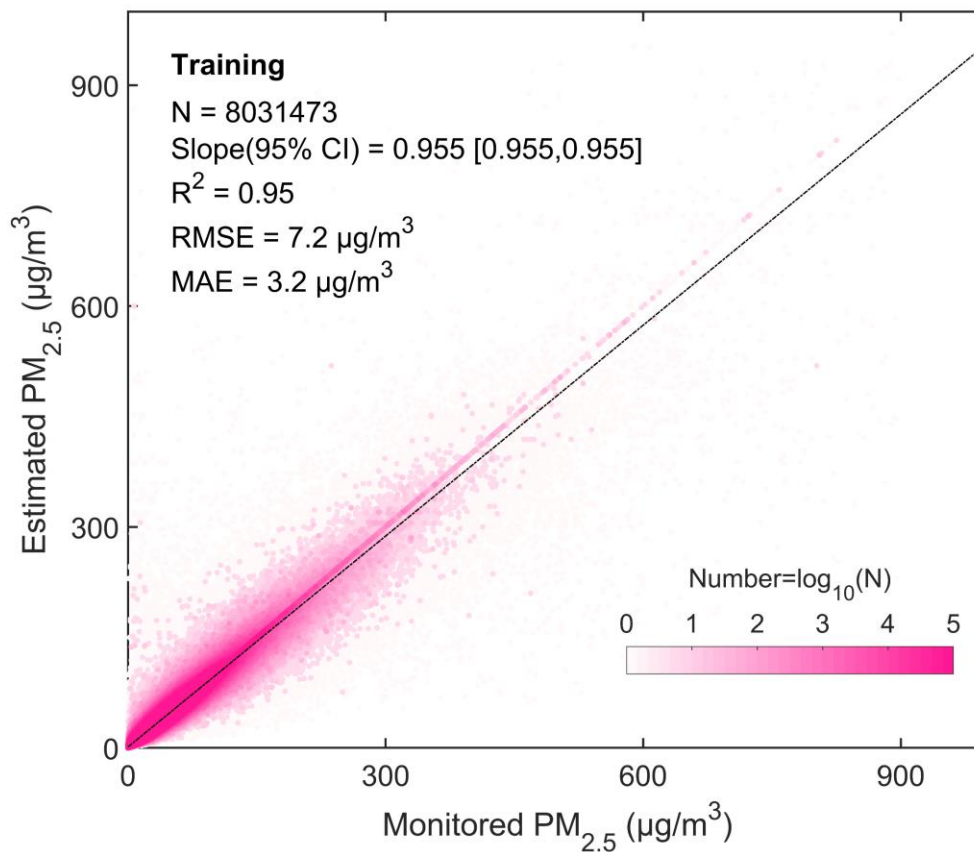
Figure 3. Density scatter plot (a) between estimated PM$_{2.5}$ concentration and monitored PM$_{2.5}$ concentration. The dashed black line is the linear regression line. N is the length of the data pairs, and Slope is the linear regression coefficient within a 95% confidence interval (CI). R^2 is the coefficient of determination, RMSE is the root mean square error, and MAE is the mean absolute error.

Figure 4 (a-c) shows the spatial distribution (a-c) and frequency of training of RMSE, MAE, and ρ. Table 2 lists the model's performance metrics in the United States, Canada, Europe, China, and India. For all sites, the average RMSE is 6.92 μg/m^3, with a median of 4.76 μg/m^3. The RMSE of 80% of the sites is less than 10.01 μg/m^3. The RRMSE (the percentage of RMSE to mean of PM$_{2.5}$ concentration) is 28.7%. The MAE is 3.77 μg/m^3, with a median of 2.72 μg/m^3. The MAE is less than 5.66 μg/m^3 for 80% of the sites. The RMAE (the percentage of MAE to mean of PM$_{2.5}$ concentration) is 15.4%. The average ρ is 0.91, and the median is 0.92. The ρ of 80% of the sites is greater than 0.87. Previous studies have shown that for PM$_{2.5}$ concentration retrieved from daily visibility or satellite aerosol optical depth, the R^2 range of the model is from 0.42 to 0.89, and the RMSE range is from 9.59 μg/m^3 to 32.09 μg/m^3 (Shen et al., 2016; Liu et al., 2017; Wei et al., 2019b; Gui et al., 2020; Li et al., 2021; Zhong et al., 2021). This finding indicates that our model performs well at the daily scale.

On the regional scale, the RMSE values for the United States, Canada, Europe, China, and India are 3.10 μg/m^3, 2.78 μg/m^3, 4.92 μg/m^3, 9.65 μg/m^3 and 17.46 μg/m^3, respectively. and the RRMSE values are 34.9%, 40.4%, 29.8%, 23.1%, and 28.8%, respectively. The MAEs for the United States, Canada, Europe, China, and India are 1.61 μg/m^3, 1.35 μg/m^3, 2.54 μg/m^3, 5.47 μg/m^3, and 9.13

μg/m³, respectively. The RMAEs are 17.9%, 19.5%, 16.3%, 13.1%, and 14.4%, respectively. The ρ values for the United States, Canada, Europe, China, and India are 0.87, 0.88, 0.91, 0.94, and 0.92, respectively. The correlation coefficients are higher in China and India, low in the United States and Canada.

The largest RMSE and MAE are in India, and the smallest are in Canada. The RRMSE and RMAE are larger in the United States, Canada and Europe than in China and India and other regions.

Table 2. The metrics for all sites and sites in the United States (the US), Canada, Europe, China and India. RRMSE is the percentage of RMSE to mean of PM$_{2.5}$ concentration. RMAE is the percentage of MAE to mean of PM$_{2.5}$ concentration.

Region	RMSE (μg/m³)	MAE (μg/m³)	ρ	Mean (μg/m³)	RRMSE (%)	RMAE (%)
All	6.92	3.77	0.91	26.7	28.7	15.4
the US	3.10	1.61	0.87	9.1	34.9	17.9
Canada	2.78	1.35	0.88	6.9	40.4	19.5
Europe	4.92	2.54	0.91	15.7	29.8	16.3
China	9.65	5.47	0.94	42.1	23.1	13.1
India	17.46	9.13	0.92	63.1	28.8	14.4
Other	6.11	3.32	0.91	23.4	24.8	14.1
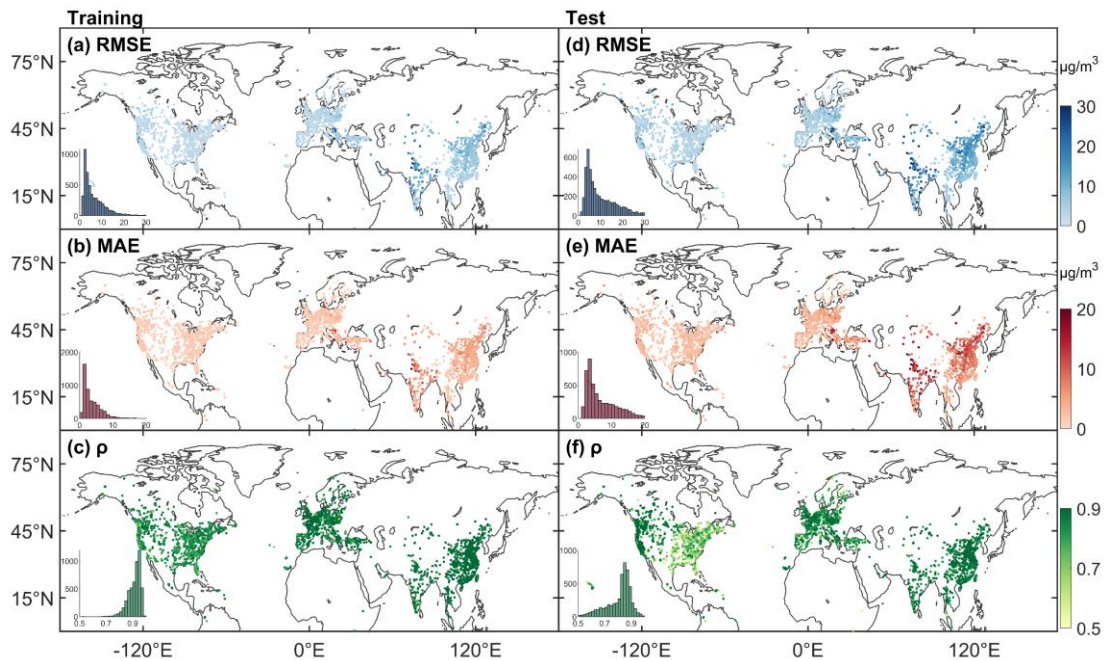
Figure 4. Statistical Metrics distribution of training (left) and test (right). The bar is the frequency of sites. RMSE is the root mean square error, MAE is the mean absolute error, and ρ is the correlation coefficient.

3.3 Evaluation of Model's Predictive Ability

A total of 1911183 pairs of test data is employed to evaluate the model's predictive ability. Figure 5 is the density scatter plot between the predicted PM$_{2.5}$ concentration and the test PM$_{2.5}$ concentration. The linear regression slope (95% CI) is 0.864 [0.863, 0.865], R^2 is 0.79, RMSE is 14.8 μg/m³, and

496   MAE is 7.6 μg/m³. Previous studies have shown that the R^2 range of the model's predictive results

497   at the daily scale is 0.31 - 0.84, and the RMSE range is 13.8-29.0 μg/m³ (Gui et al., 2020; Zhong et

498   al., 2021). The test results exhibit excellent predictive capability.
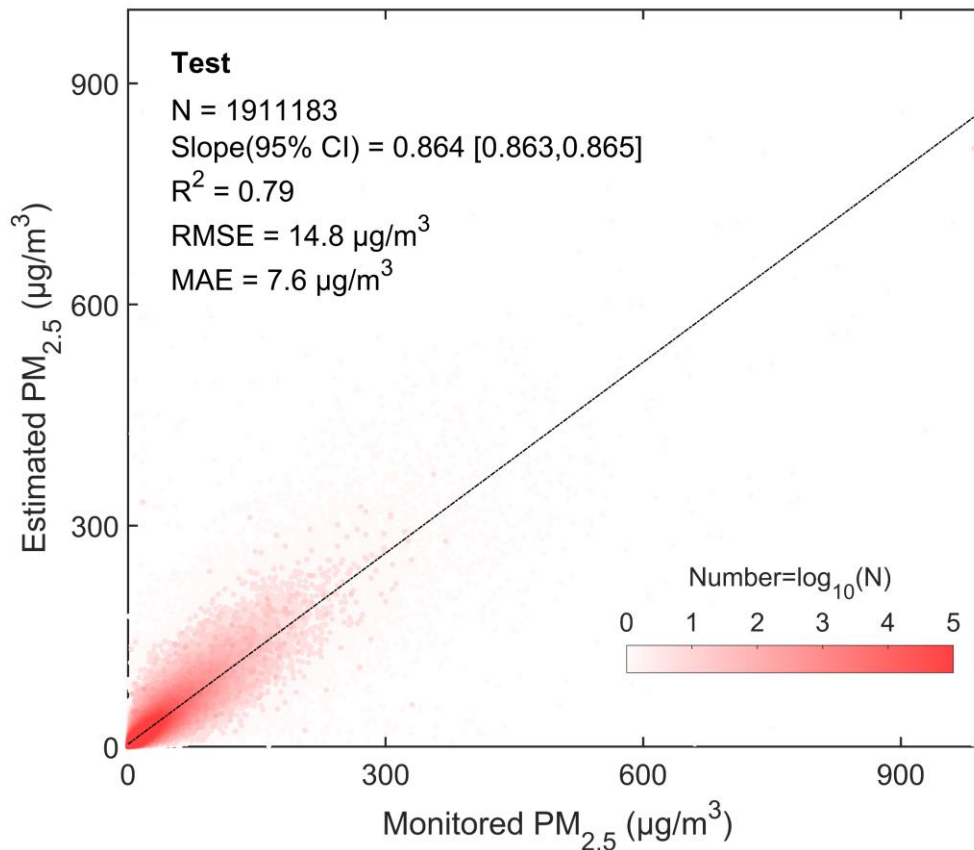
499

500   **Figure 5**. Density scatter plot (a) between the predicted $PM_{2.5}$ concentration and monitored $PM_{2.5}$

501   concentration of the test results. The dashed black line is the linear regression line. N is the length

502   of the data pairs, and Slope is the linear regression coefficient within a 95% confidence interval (CI).

503   R^2 is the coefficient of determination, RMSE is the root mean square error, and MAE is the mean

504   absolute error.

505   We analyze the test results for Canada, the United States, Europe, China, and India to assess the

506   predictive ability of the model in different regions. Figure 4 (d - f) shows the spatial distributions of

507   the test RMSE, MAE, and ρ and their frequency. Table 3 lists the test results of the metrics. For all

508   sites, the average RMSE is 11.50 μg/m³. The RRMSE is 46.0%. The average MAE is 7.72 μg/m³.

509   The RMAE is 30.7%. The ρ is 0.81. For the United States, the RMSE, MAE, and ρ are 5.06 μg/m³,

510   3.25 μg/m³, and 0.72, respectively. For Canada, the RMSE, MAE, and ρ are 4.73 μg/m³, 2.88 μg/m³,

511   and 0.77, respectively. The results in the United States and Canada are better in the west than in the

512   east. The RMSE, MAE, and ρ for Europe are 7.79 μg/m³, 5.10 μg/m³, and 0.80, respectively. For

513   China, the RMSE, MAE, and ρ are 16.83 μg/m³, 11.50 μg/m³, and 0.85, respectively. For India, the

514   RMSE, MAE, and ρ are 27.05 μg/m³, 17.89 μg/m³, and 0.85, respectively. The results show that in

515   developing regions (China and India), ρ is better than that in developed regions (the United States,

516   Canada, and Europe), which means that the predictive ability of the model is better for severely

517   polluted regions.

Table 3. The test results of the model's performance metrics for all sites and sites in the United States, Canada, Europe, China and India. RRMSE is the percentage of RMSE to mean of PM$_{2.5}$ concentration. RMAE is the percentage of MAE to mean of PM$_{2.5}$ concentration.

Region	RMSE ($\mu g/m^3$)	MAE ($\mu g/m^3$)	ρ	Mean ($\mu g/m^3$)	RRMSE (%)	RMAE (%)
All	11.50	7.72	0.81	27.1	46.0	30.7
the US	5.06	3.25	0.72	9.4	54.3	35.0
Canada	4.73	2.88	0.77	7.2	65.6	40.0
Europe	7.79	5.10	0.80	15.9	47.0	32.0
China	16.83	11.50	0.85	42.6	39.6	27.1
India	27.05	17.89	0.85	63.7	42.9	27.8
Other	8.86	6.16	0.81	23.4	36.7	26.1

3.4 Uncertainties and Limitations

3.4.1 Uncertainty in the Pollution Level

Figure 6 shows the uncertainty in the predicted PM$_{2.5}$ concentration with respect to the pollution level of the monitored PM$_{2.5}$ concentration. For all sites, the uncertainty in the bias increases as the pollution level increases. The mean and median of the bias shift from positive to negative with increasing pollution levels. 83.6% of PM$_{2.5}$ concentration data is less than 45 $\mu g/m^3$, and the mean bias (< 0.8 $\mu g/m^3$) is positive. 36.8% is less than 10 $\mu g/m^3$, and the median (< 0.4 $\mu g/m^3$) of the bias is positive. 16.4% of PM$_{2.5}$ concentration is great than 45 $\mu g/m^3$, and the mean bias is negative. 63.2% of PM$_{2.5}$ concentration is great than 10 $\mu g/m^3$, and the median is negative. It indicates that the model overestimates at low pollution level and underestimates at high pollution level.

The bias for each region also increases with pollution level. For the United States, the mean bias of 69.4% is positive and less than 0.8 $\mu g/m^3$, and the PM$_{2.5}$ concentration is less than 10 $\mu g/m^3$. When the PM$_{2.5}$ concentration is greater than 10 $\mu g/m^3$, the mean bias is negative. For Canada, the mean bias of 74.1% is positive and less than 0.7 $\mu g/m^3$. When the PM$_{2.5}$ concentration is greater than 8 $\mu g/m^3$, the mean bias is negative. For Europe, the mean bias of 67.1% is positive and less than 0.9 $\mu g/m^3$. When the PM$_{2.5}$ concentration is greater than 15 $\mu g/m^3$, the mean bias is negative. For China, 67.7% of the bias is positive and less than 2.7 $\mu g/m^3$. When the PM$_{2.5}$ concentration is greater than 45 $\mu g/m^3$, the mean bias is negative. For India, 80.1% of the bias is positive and less than 4.2 $\mu g/m^3$, and when the PM$_{2.5}$ concentration is greater than 100 $\mu g/m^3$, the mean bias is negative. When the PM$_{2.5}$ concentration is greater than 60 $\mu g/m^3$, the bias median is negative, with a percentage of 40.3%. The uncertainty in each region is similar, and the uncertainty increases as the pollution level increases.

543
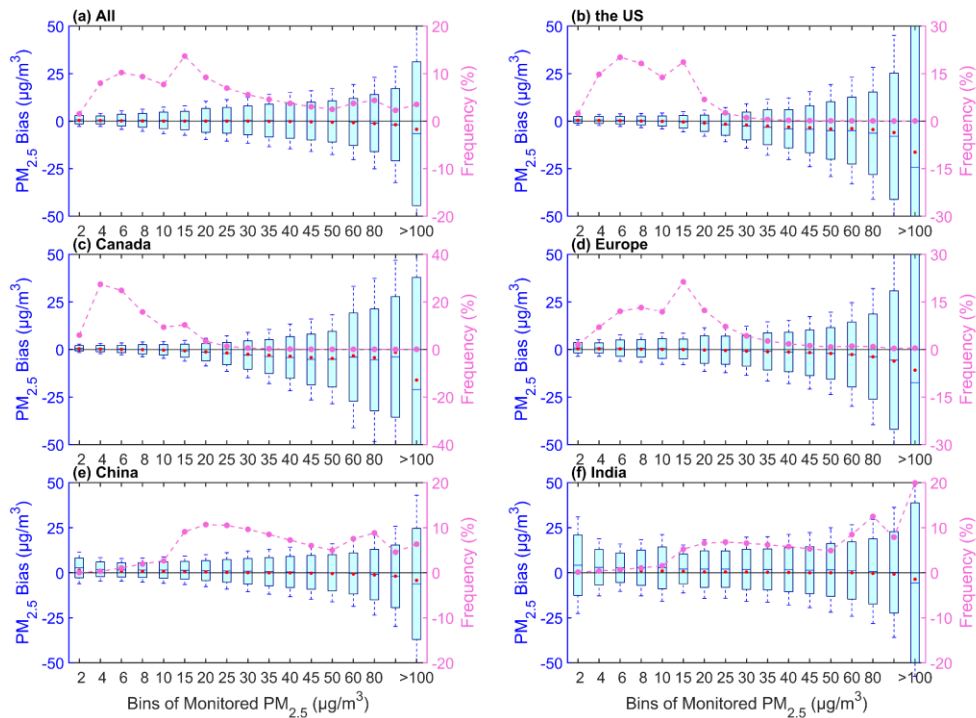
Figure 6. Boxplots of the pollution level and bias (predicted PM$_{2.5}$ concentration - monitored PM$_{2.5}$ concentration) for all sites (a), sites in the United States (b), Canada (c), Europe (d), China (e), and India (f). The box's upper and lower limits represent ± 1 standard deviation, the whiskers represent 2 times the standard deviation, the red circle represents the median, and the short line represents the mean bias. The frequency (%) on the right y-axis represents the percentage of data with different pollution levels (dashed line).

3.4.2 Uncertainty in the Station Elevation

With the spatial variability in PM$_{2.5}$ concentration, we analyze the mean bias at different visibility station elevations. Figure 7 shows the relationships between the elevations of the visibility stations and the bias. The bias exhibits variations across different elevations for all stations. The mean bias of all sites ranges from -0.04 to 0.02 μg/m³. A total of 90.1% of the stations has positive biases. The median of the bias is almost positive, with a positive bias of 99.5% stations, except for the elevation at 4 km. The elevations of 86.5% of the stations are less than 1 km, with a positive median of the bias. High uncertainties in bias occur at elevations of 0.05 km, 0.2 km, and 0.3 km. Negative biases are observed at elevations of 0.4 km, 0.9-1 km, and 4 km. This finding indicates a nonsignificant overestimation of the predicted PM$_{2.5}$ concentration due to the various elevations.

The bias patterns vary across regions. For the United States, a total of 88.8% of the stations have negative biases. The median of the bias is negative with a percentage of 63.4%. High uncertainties in bias occur at elevations of 0.05 km, 2 km, and 0.3 km. For Canada, 52.3% of the stations have positive biases. The median of the bias is negative with a percentage of 33.8%. High uncertainties in bias occur at elevations of 0.05 km and 1 km. For Europe, 58.9% of the stations have positive biases. The median of the bias is negative with a percentage of 40.2%. High uncertainties in bias occur at elevations of 0.05 km and 0.9 km. For China, 76.7% of the stations have negative biases.

The median of the bias is negative with a percentage of 54.1%. High uncertainties in bias occur at elevations of 0.05 km, 0.5 km and 3 km. For India, 68.1% of the stations have positive biases. The median of the bias is negative with a percentage of 63.8%. The elevation of most stations with a high uncertainty is at 0.05 km. High uncertainties in bias occur at elevations of 0.1 km and 3 km. More stations with negative bias are in the United States and China. More stations with positive bias are in Canada, Europe and India.
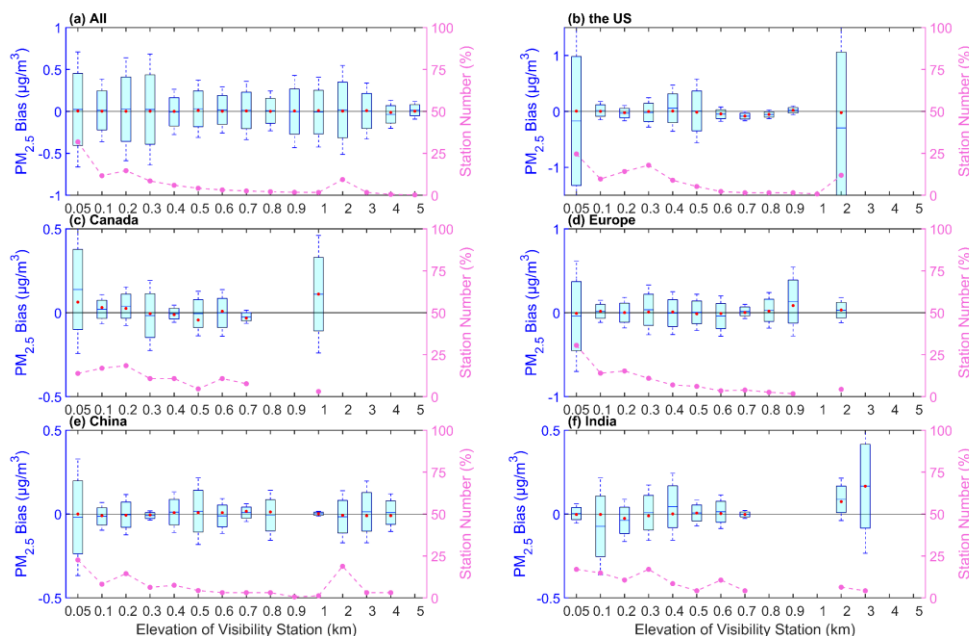
Figure 7. Boxplots of the bias (predicted PM$_{2.5}$ concentration - monitored PM$_{2.5}$ concentration) and the elevation of the visibility station for all sites (a), sites in the United States (b), Canada (c), Europe (d), China (e), and India (f). The box's upper and lower limits represent ± 1 standard deviation, the whiskers represent 2 times the standard deviation, the red circle represents the median, and the short line represents the mean bias. The station number (%) on the right y-axis represents the percentage of station number at different elevations (dashed line).

3.4.3 Uncertainty in the Station Distance

As the visibility stations and PM$_{2.5}$ sites are not collocated, we analyze the mean bias of PM$_{2.5}$ concentration at different distances, as shown in Figure 8. For all sites, 86.1% of the stations have negative biases. The median of the bias is negative with a percentage of 70.8%. More stations have a negative bias caused by the distance. The uncertainty has no signification with the distance. The distances with low uncertainties are at 1 km and 20-40 km. The distances with high uncertainties are at 5 km and 60 km.

For the United States, 63.1% of the stations have negative biases. The median of the bias is negative with a percentage of 69.2%. The distance with the lowest uncertainty is at 1 km. The distances with high uncertainties are at 5 km and 60 km. For Canada, 60.0% of the stations have positive biases. The median of the bias is positive with a percentage of 80.0%. The uncertainty shows an increase with the distance increasing. For Europe, 72.7% of the stations have negative biases. The median of the bias is positive with a percentage of 67.1%. When the distance is less than 10 km, the uncertainty

increases with the distance. The distances with low uncertainties are at 1 km and 30-40 km. The distances with high uncertainties are at 10 km and 75 km. For China, 64.3% of the stations have negative biases. The median of the bias is negative with a percentage of 72.7%. The distance with a low uncertainty is at 30 km. The distance with a high uncertainty is at 60 km. For India, 62.3% of the stations have negative biases. The median of the bias is positive with a percentage of 59.1%. The distance with the lowest uncertainty is at 30 km. The distance with the highest uncertainty is at 20 km.

More visibility stations have negative biases, except for the stations in Canada. For the stations in the United States, Canada and Europe, the lowest uncertainty is at 1 km. For the stations in China and India, the uncertainty has no significant relationship with distance, though the distance has caused a negative bias.
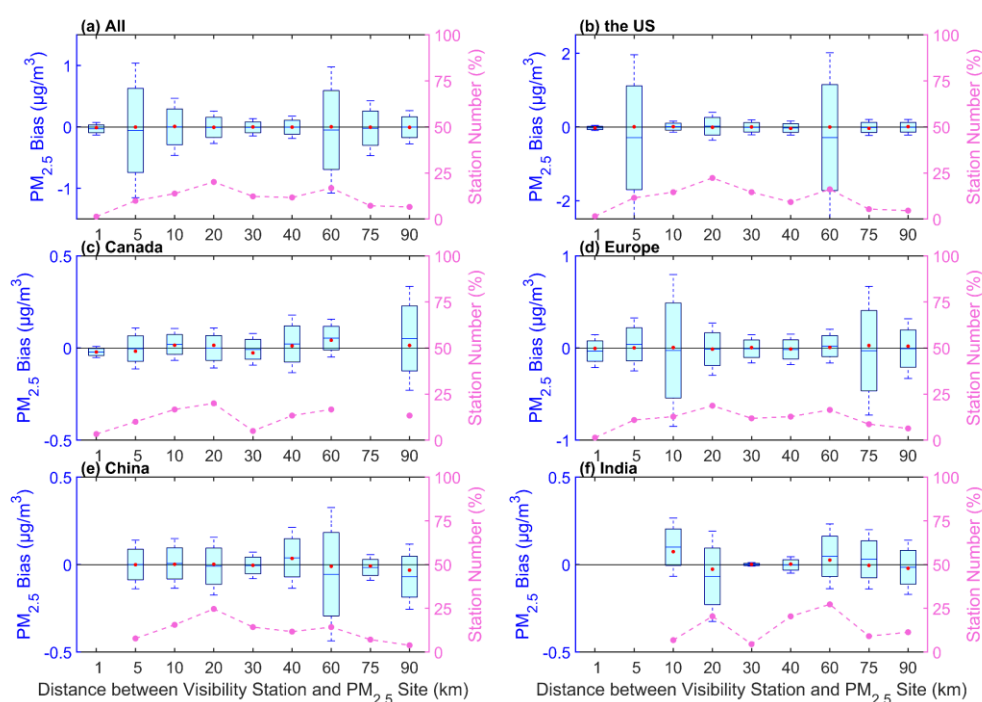
Figure 8. Boxplots of the mean bias (predicted PM$_{2.5}$ concentration - monitored PM$_{2.5}$ concentration) and the distance between the visibility station and the PM$_{2.5}$ site and for all sites (a), sites in the United States (b), Canada (c), Europe (d), China (e), and India (f). The box's upper and lower limits represent ±1 standard deviation, the whiskers represent 2 times the standard deviation, the red circle represents the median, and the short line represents the mean bias. The station number (%) on the right y-axis represents the percentage of station number under different distances (dashed line).

3.4.4 Discussion on the Uncertainties and Limitations

There are some uncertainties and limitations in this study. The upper limit of visibility and PM$_{2.5}$ concentration can cause some uncertainties in model training. The maximum distance between the visibility stations and PM$_{2.5}$ monitoring sites is 100 km due to the spatial variability in aerosols, which may increase the uncertainty in the estimated PM$_{2.5}$ concentration. Because of the nonuniform vertical distribution of aerosols, the different elevations of the visibility stations and the PM$_{2.5}$ monitoring sites further increase the uncertainty in estimating PM$_{2.5}$ concentration. In addition, the

spatial coverage of visibility stations, especially in China and India, is still limited, which may increase the uncertainty in the representativeness of regional $PM_{2.5}$ concentration and pollution levels. With the increasing human concern of air pollution and the implementation of air pollution control measures, the types of major atmospheric pollutants may have changed at regional scale, the composition of particulate matter has also evolved, the scattering and absorption characteristics may have changed, and the relationship between visibility and $PM_{2.5}$ concentration may change. These changes may lead to uncertainties in estimating historical $PM_{2.5}$ concentration. It is challenging to validate by ground observations and satellite-based estimation prior to 2000. Despite these limitations and challenges, we establish a long-term $PM_{2.5}$ concentration dataset based on visibility from 1959 to 2022, which has been carefully validated and evaluated, providing insights into the long-term spatiotemporal characteristics of concentration $PM_{2.5}$ in the Northern Hemisphere.

4 Comparisons with Other $PM_{2.5}$ Concentration Dataset

We compare the daily and monthly estimated $PM_{2.5}$ concentration with the LGHAP $PM_{2.5}$ concentration from 2000 to 2021 to further demonstrate the reliability the estimated $PM_{2.5}$ concentration. When comparing on the regional scale, we split the time range into 2000-2010 and 2011-2021, to further validate the accuracy and consistency of estimated $PM_{2.5}$ concentrations, as in some regions such as India and China, there are almost no continuous $PM_{2.5}$ monitoring data before 2010.

4.1 Comparisons on the Daily Scale

We spatiotemporally match the LGHAP $PM_{2.5}$ concentration with the estimated $PM_{2.5}$ concentration. Figure 9 shows the density scatter plot between the estimated $PM_{2.5}$ concentration and LGHAP $PM_{2.5}$ concentration. There is a total of 96188682 pairs during the period of 2000 and 2021, 46846389 pairs during the period from 2000 to 2010, and 49342302 during the period of 2011 and 2021, with slopes of 0.817, 0.758 and 0.867. The intercepts are 6.928 $\mu g/m^3$, 8.933 $\mu g/m^3$, and 5.377 $\mu g/m^3$, respectively. The slope decreases before 2010, which may be related to the upper limit of LGHAP $PM_{2.5}$ concentration with a significantly decreasing quantity of the concentration (> 300 $\mu g/m^3$).

We further compare the $PM_{2.5}$ concentrations of the annual calendar cycles on the regional scale in Figure 10. The $PM_{2.5}$ concentration of each day is the mean of the $PM_{2.5}$ concentrations at all sites in the region. The correlation coefficients of the $PM_{2.5}$ concentrations are greater than 0.89 from 2011 to 2021 and greater than 0.92 from 2000 to 2010. The correlation is greater in Europe, China, and India than in the United States and Canada. There is no significant difference in the variation of annual calendar cycles between two periods on the regional scale. In the United States, $PM_{2.5}$ concentration between 2000 and 2010 is more similar than the concentration between 2011 and 2021, and the bias decreases. In Canada, the correlation coefficient increases, although the bias increases. In Europe, the correlation coefficient and bias increase. There are similar changes in China and India. The bias increases on days 1 to 60 and 300 to 366, but the correlation remains significant. The difference of $PM_{2.5}$ concentration during the two periods is mainly reflected in the increasing bias in Canada and Europe, which is a non-seasonal bias and the increasing bias in winter in China and India, which is a seasonal bias. Overall, $PM_{2.5}$ concentrations show a good consistency before and after 2010 on the daily scale.
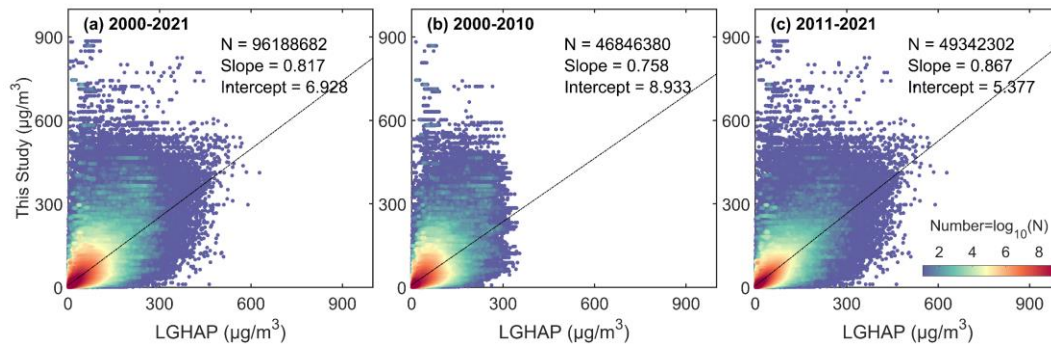
659

660 **Figure 9**. Density scatter plot between the estimated PM$_{2.5}$ concentration (this study) and LGHAP
661 PM$_{2.5}$ concentration on the daily scale from 2000 to 2021 (a), from 2000 to 2010 (b) from 2011 to
662 2021. The dashed black line is the linear regression line. N is the length of the data pairs, and Slope
663 is the linear regression coefficient. Intercept represents the y-intercept.
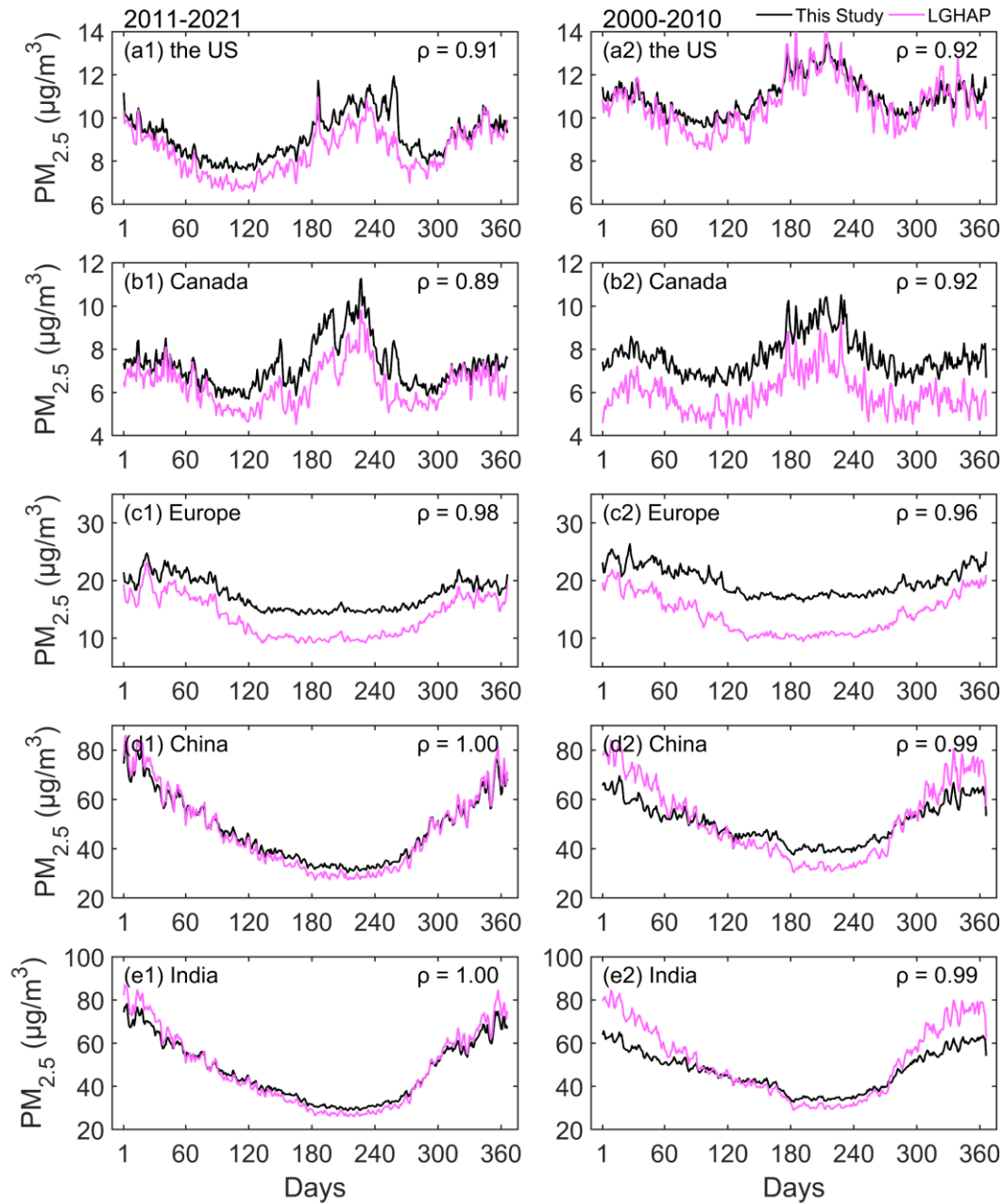
Figure 10. Comparison of annual calendar cycle of PM$_{2.5}$ concentration on the regional scale from 2011 to 2021 (left) and from 2000 to 2010 (right) between the estimated PM$_{2.5}$ concentration (this study) and LGHAP PM$_{2.5}$ concentration on the daily scale. ρ is the correlation coefficient.

4.2 Comparisons on the Monthly Scale

Figure 11 shows the density scatter plot between the estimated PM$_{2.5}$ concentration and LGHAP PM$_{2.5}$ concentration on the monthly scale. The monthly PM$_{2.5}$ concentration is calculated by the matched daily concentrations. There is a total of 3296739 pairs during the period from 2000 to 2021, 1582161 pairs during the period from 2000 to 2010, and 1714578 during the period from 2011 to 2021, with slopes of 0.857, 0.821 and 0.879. The intercepts are 6.774 μg/m^3, 8.716 μg/m^3, and 5.272 μg/m^3, respectively. The slope of monthly concentration significantly improves before 2010, and slightly increases after 2010 compared to the daily scale.

676   We also compare the $PM_{2.5}$ concentrations of the annual cycles on the regional scale in Figure 12.

677   The $PM_{2.5}$ concentration of each month is the mean of the $PM_{2.5}$ concentrations at all sites in the

678   region. The correlation coefficients of the $PM_{2.5}$ concentrations are greater than 0.92 from 2011 to

679   2021 and greater than 0.87 from 2000 to 2010. In the United States, the $PM_{2.5}$ concentrations before

680   2010 are closer compared to those after 2010, except in April and August, and the biases in other

681   months has significantly decreased. In Europe and Canada, the biases have increased. In China, the

682   result is similar with the result on the daily scale. In India, the performance of the two is almost

683   consistent, with a correlation coefficient of 0.99 and 0.96. The two datasets have a very high

684   similarity in annual cycles, indicating that the estimated $PM_{2.5}$ concentration in this study is accurate

685   and consistent before and after 2010.
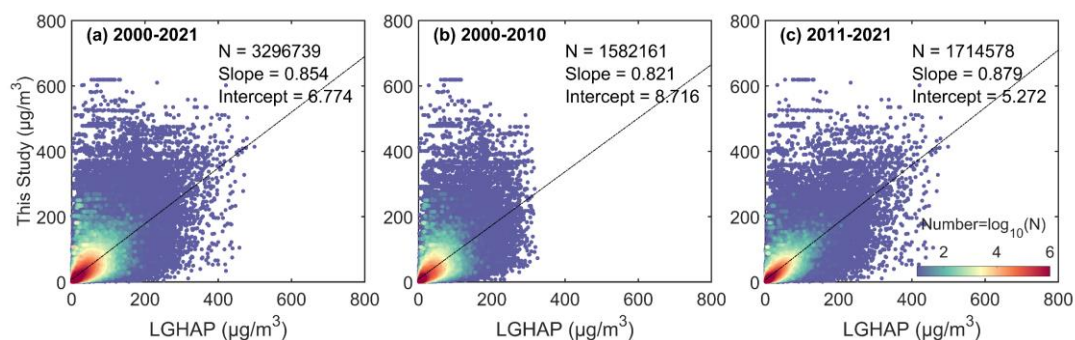
686

687   **Figure 11**. Density scatter plot between the estimated $PM_{2.5}$ concentration (this study) and LGHAP

688     $PM_{2.5}$ concentration on the monthly scale from 2000 to 2021 (a), from 2000 to 2010 (b) from 2011

689   to 2021. The dashed black line is the linear regression line. N is the length of the data pairs, and

690   Slope is the linear regression coefficient. Intercept represents the y-intercept.

691
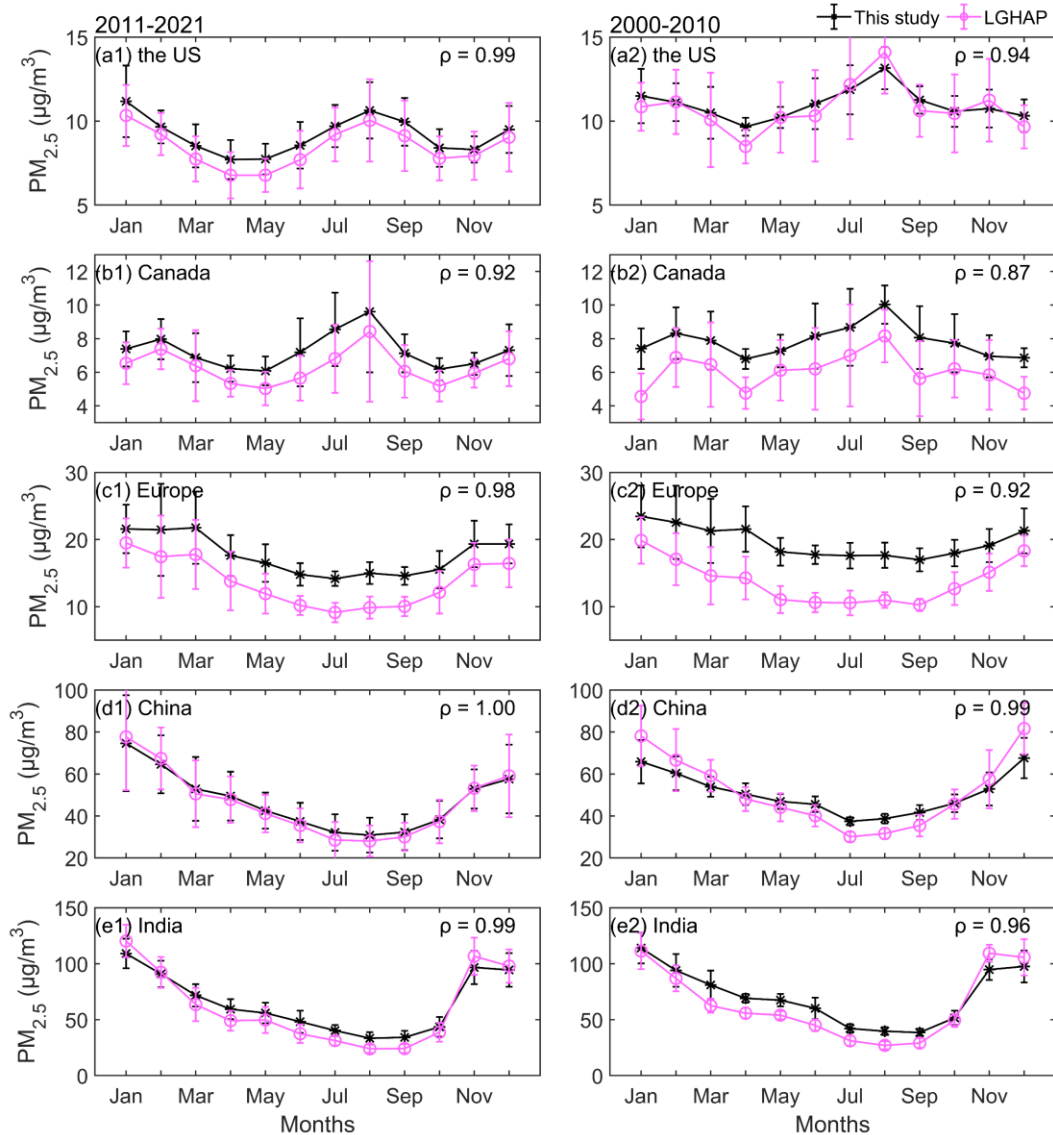
Figure 12. Comparison of annual cycle of monthly PM$_{2.5}$ concentration on the regional scale from 2011 to 2021 (left) and from 2000 to 2010 (right) between the estimated PM$_{2.5}$ concentration (this study) and LGHAP PM$_{2.5}$ concentration on the daily scale. ρ is the correlation coefficient.

4.3 Discussion on the Differences of PM$_{2.5}$ Concentration from Visibility and Aerosol Optical Depth

Both visibility and aerosol optical depth are excellent alternatives for estimating PM$_{2.5}$ concentration, with its own advantages. However, they have differences in principle, which may be the reason for the difference between the two datasets in comparison.

Fine particulate matter near the ground surface affects atmospheric visibility through scattering. Studies have shown visibility has a negative correlation with PM$_{2.5}$ concentration, and the reciprocal of visibility has a positive correlation with the extinction coefficient and has a negative correlation with the particulate matter concentration (Wang et al., 2012; Zhang et al., 2017; Zhang et al., 2020). Therefore, visibility is often used as a proxy for particulate matter pollution (Huang et al., 2009; Singh et al., 2020) and it is the basis to estimate PM$_{2.5}$ concentration. In addition, studies have shown

706 that meteorological observations such as temperature and humidity also play an important role in
707 estimating $PM_{2.5}$ concentration using visibility (Shen et al., 2016; Xue et al., 2019; Zhong et al.,
708 2021). Therefore, when estimating $PM_{2.5}$ concentration based on visibility data, only conventional
709 meteorological variables need to be added, which is convenient and accurate observational data.
710 Besides, the long-term, complete and high-temporal ground-based observations are the advantage
711 of historical estimation of $PM_{2.5}$ concentration. The daily mean from continuous or equidistant
712 hourly observations greatly increases the daily representativeness.

713 The aerosol optical depth is a physical quantity that describes aerosol column properties, which is
714 the integration of the extinction coefficient in the vertical direction. When establishing a connection
715 between aerosol optical depth and near-ground $PM_{2.5}$ concentration, it is essential to consider the
716 vertical structure of aerosols. Studies have shown that the aerosol vertical profiles usually are
717 provided by observations, assumptions, or chemical transport models to obtain the aerosol
718 properties near the surface (Van Donkelaar et al., 2010; Wei et al., 2019b; Van Donkelaar et al.,
719 2021). Van Donkelaar et al. (2006; 2010) have demonstrated that aerosol vertical profile errors in
720 chemical transport models and aerosol optical depth retrieval and sampling result in an
721 approximately 25% uncertainty of one standard deviation. Sensitivity testing shows that a 1%
722 estimation error in the aerosol optical depth can lead to a 0.27% estimation error in the $PM_{2.5}$
723 concentration (Wei et al., 2021). Besides, the retrieval of aerosol optical depth is affected by clouds
724 or surface types and a finite number of daily observations (usually 1-2 times), though it has the
725 advantage of high spatial coverage (Liu et al., 2017; Singh et al., 2020; Zhong et al., 2021).

726 Another difference is the upper limit of $PM_{2.5}$ concentration. In this study, the upper limit of the
727 estimated daily $PM_{2.5}$ concentration is set to 1000 μg/m³ (the same for input data). When the $PM_{2.5}$
728 concentration is greater than 500 μg/m³ during heavy pollution, which may contribute to the higher
729 frequency at high pollution levels than in the LGHAP dataset, especially before 2010. We do not
730 remove visibility records during dust weather when preprocessing the data, which may lead to an
731 overestimation of $PM_{2.5}$ concentration in dusty areas, such as northern China and northwestern India.
732 In section 3.4, the uncertainty analysis has provided an explanation for the overestimation. Overall,
733 our $PM_{2.5}$ concentration dataset has a good consistency with $PM_{2.5}$ concentration based on aerosol
734 optical depth.

5 Regional Trends and Spatial Patterns

736 We use the estimated $PM_{2.5}$ concentrations (at least 10-day records in a site) to calculate monthly
737 $PM_{2.5}$ concentrations, and analyze the annual cycles, interannual trends, and spatial patterns of $PM_{2.5}$
738 concentrations in different regions based on the GAMM model. The annual variation comes from
739 the monthly smooth term of GAMM, the interannual variation comes from the annual smooth term,
740 and the spatial pattern comes from the spatial smooth term. The regions include Canada, the United
741 States, Europe, China, and India. The results are shown in Figure 13. The trend from 1959 to 2022
742 in each region is the slope of the Sen-Theil (ST Slope) estimators (Sen, 1968; Theil, 1992), and
743 Mann-Kendall test (Mann, 1945; Kendall, 1948) is used to calculate the significance of the trend.
744 The test results show the p-values are all less than 0.01 in all regions.

745 In the United States, the annual cycle curve shows that the $PM_{2.5}$ concentration is a 'double peaks
746 and double valleys' shape. The peaks occur in July and December, respectively, with the highest
747 $PM_{2.5}$ concentration in July throughout the year. The valley values are in April and October, and the

748   PM$_{2.5}$ concentration levels are equivalent. The trend is -0.40 μg/m^3/decade, and PM$_{2.5}$ concentration
749   decreases significantly after 1992, with a trend of -1.39 μg/m^3/decade. The high PM$_{2.5}$ concentration
750   areas are in the east and west. The areas with low PM$_{2.5}$ concentrations are mainly located in the
751   central and northern regions. The high concentration in the eastern and western regions is related to
752   extensive industrial activities and densely populated cities. The low concentration in the central and
753   northern regions is relatively to high vegetation coverage, low industrial activity and low population
754   density.

755   In Canada, the annual cycle curve also shows that the PM$_{2.5}$ concentration is a 'double peaks and
756   double valleys' shape. The peak values occur in August and February, with the highest PM$_{2.5}$
757   concentration in August. The valley values are in April and October. The trend is -0.10 μg/m^3/decade,
758   and PM$_{2.5}$ concentration increases after 2010. The PM$_{2.5}$ concentration exhibits an east-high to west-
759   low pattern. The eastern regions, such as Ontario and Quebec, are characterized by high population
760   density and significant industrial and transportation activities.

761   In Europe, the annual cycle of PM$_{2.5}$ concentration shows that the PM$_{2.5}$ concentration is the highest
762   in February, and is low from May to September. The valley values are in April and October. The
763   trend is -1.55 μg/m^3/decade. High concentration areas are distributed in eastern Europe, while low
764   concentration areas are in northern and western Europe. Eastern Europe exhibits more
765   industrialization, particularly with a prevalence of traditional heavy industries and the use of coal
766   and other high-pollution energy sources. In contrast, the energy structure in western Europe tends
767   to favor cleaner energy sources.

768   In China, the annual cycle curve of PM$_{2.5}$ concentration presents a V-liked shape. It indicates that
769   high concentrations are in winter, while low concentrations are in summer. The trend is 2.09
770   μg/m^3/decade. The trend is 2.65 μg/m^3/decade from 1959 to 2011 and -22.23 μg/m^3/decade from
771   2012 to 2022. High concentration areas are distributed in northern China, such as North China Plain,
772   Northeast China, Sichuan Basin, Taklimakan Desert, and Badain Jaran Desert. Low concentration
773   areas are in southern China and Northern Tianshan Mountains. Besides dust, industrial activities
774   and coal combustion for heating during winter are significant contributors to the PM$_{2.5}$ concentration
775   in northern regions.

776   In India, the annual cycle curve of PM$_{2.5}$ concentration also presents a V-liked shape. High
777   concentrations are in winter, and low concentrations are in summer. The trend is 0.92 μg/m^3/decade.
778   The trend is 1.41 μg/m^3/decade from 1959 to 2013 and -23.36 μg/m^3/decade from 2014 to 2022.
779   Some studies have shown that the PM$_{2.5}$ concentration in India has decreased since 2014, especially
780   in northern cities. Singh et al. (2021) have found that five major cities in India show a downward
781   trend from 2014 to 2019, with the largest decline of approximately -4.2 μg/m^3 per year in New Delhi.
782   Ravindra et al. (2024) also finds that the trend in New Delhi is about -5 μg/m^3 per year from 2014
783   to 2020. These studies have shown a faster downward trend than our study, as these PM$_{2.5}$
784   monitoring sites are mainly concentrated in urban areas. The PM$_{2.5}$ concentration exhibits a north-
785   high to south-low pattern. High concentration areas are distributed in northern India, such as Ganges
786   Plain and Thar Desert, because there are more industrial and densely populated areas and the terrain
787   leads to the retention of air pollutants. Low concentration areas are in Deccan Plateau.

788   Above all, the PM$_{2.5}$ concentrations in developed countries and regions are significantly lower than
789   those in developing countries in the Northern Hemisphere. Regional trends are similar with those

790 of previous studies in different periods (Van Donkelaar et al., 2010; Wang et al., 2012; Boys et al.,
791 2014; Ma et al., 2016; Li et al., 2017; Hammer et al., 2020). The trends in $PM_{2.5}$ concentration
792 changes in different regions are closely associated with the implementation of relevant policies. The
793 earlier pollution control measures are taken, the earlier the decreasing trend in the $PM_{2.5}$
794 concentration occurs, and the lower the threat of particulate matter pollution is to humans. In 1997,
795 the United States EPA classified $PM_{2.5}$ as a hazardous substance in the National Ambient Air Quality
796 Standard, and subsequent regulations in 2006 further strengthened the source control and
797 management of fine particulate matter (Hall and Gilliam, 2016). In 1988, the Canadian federal
798 government enacted the Canadian Environmental Protection Act, which enhanced the regulation of
799 $PM_{2.5}$ (Davies, 1988). The European Union introduced the Air Quality Directive in 1996, followed
800 by multiple revisions and updated to regulate and restrict air pollutants, including $PM_{2.5}$ (Kuklinska
801 et al., 2015). However, Europe stands out due to its early adoption of clean production practices in
802 heavy industries since the 1970s. Since 2012, China has implemented numerous regulations and
803 standards for $PM_{2.5}$. For instance, the Monitoring Method for Atmospheric Particulate Matter ($PM_{2.5}$)
804 was issued in 2012, and the Chinese Ministry of Environmental Protection released the Ambient Air
805 Quality Standards in 2013, including emission standards for $PM_{2.5}$ (Zhao et al., 2016a). In 2009, the
806 Indian Ministry of Environment and Forests issued the National Ambient Air Quality Standards,
807 which include control standards for $PM_{2.5}$. Since 2015, the Indian government has launched the
808 National Clean Air Programme (NCAP) to improve air quality by implementing a series of measures
809 to reduce the emissions of $PM_{2.5}$ and other pollutants (Ganguly et al., 2020). These environmental
810 regulations have contributed significantly to the decline of $PM_{2.5}$ concentrations. Some studies have
811 shown that the variation of $PM_{2.5}$ concentrations is also related to several factors, such as the energy
812 structure, urbanization process, population distribution and vegetation coverage (Shi et al., 2018;
813 Wu et al., 2018; Li et al., 2019; Wang et al., 2019; Lim et al., 2020; Qi et al., 2023).

814
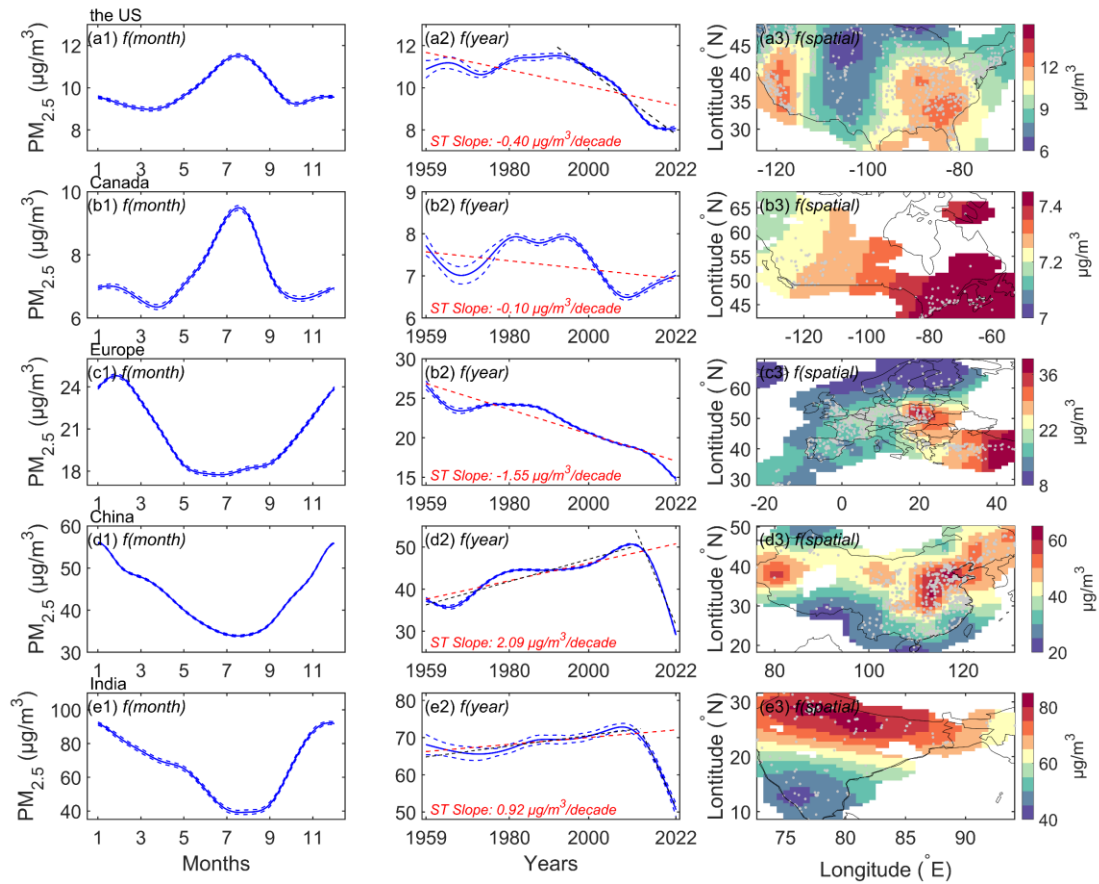
Figure 13. Annual cycles, interannual trends and spatial patterns of PM$_{2.5}$ concentrations in the United States (a1-a3), Canada (b1-b3), Europe (c1-c3), China (d1-d3), and India (e1-e3). The left column 'f(month)' is the annual cycle, the middle column 'f(year)' is the interannual trend, and the right column 'f(spatial)' is the spatial distribution from Generalized Additive Mixed Model (GAMM). The blue dashed lines represent ± 1 standard error of the month and annual mean of PM$_{2.5}$ concentrations. The red or black dashed lines represent the trends of the Sen-Theil estimators (ST Slope). Mann-Kendall test of trends shows that the p-values are less than 0.01 in all regions. The scatter points in right column are the locations of PM$_{2.5}$ monitoring sites.

6 Conclusions

In this study, we use a machine learning method to estimate daily PM$_{2.5}$ concentration for 5023 terrestrial sites in the Northern Hemisphere from 1959 to 2022 based on daily visibility and related meteorological variables. The first 80% of PM$_{2.5}$ concentration data in each site are used to train the model, and the last 20% are used to test. The model's performance and predictive ability are evaluated and a dataset of daily PM$_{2.5}$ concentration based on aerosol optical depth is used to compare and evaluate the estimated PM$_{2.5}$ concentration. We analyze the uncertainty and discuss the limitations of our dataset. Finally, the PM$_{2.5}$ concentration variation (annual calendar cycle, interannual cycle and spatial distribution) in 5 regions over the past 64 years is analyzed based on GAMM. We hope our dataset will be useful for studying the atmospheric environment, human health, and climate change and provide auxiliary support for assimilation. Several key results of this study are described as follows:

The most important variable. Visibility is the most important variable at 80.7% of the PM$_{2.5}$ sites, as visibility can be considered an indicator of PM$_{2.5}$ concentration without fog or precipitation. Other meteorological variables play a secondary role in the model, especially temperature and dew point temperature.

Model performance and predictive ability. The training results show that the slope between the estimated PM$_{2.5}$ concentration and the monitored PM$_{2.5}$ concentration within the 95% confidence interval is 0.955, the R^2 is 0.95, the RMSE is 7.2 μg/m^3, and the MAE is 3.2 μg/m^3. The test results show that the slope between the predicted PM$_{2.5}$ concentration and the monitored PM$_{2.5}$ concentration is 0.864 ± 0.0010 within a 95% confidence interval, R^2 is 0.79, RMSE is 14.8 μg/m^3, and MAE is 7.6 μg/m^3. The model shows good stability and predictive ability. Compared with a global PM$_{2.5}$ concentration dataset based on satellite retrieval, the slopes of linear regression on the daily (monthly) scale are 0.817 (0.854) from 2000 to 2021, 0.758 (0.821) from 2000 to 2010, and 0.867 (0.879) from 2011 to 2022. The result indicates the accuracy of the model and the consistency of the estimated PM$_{2.5}$ concentration on the temporal scale.

Regional trends and spatial patterns. The interannual trends and spatial patterns of PM$_{2.5}$ concentration on the regional scale from 1959 to 2022 are analyzed based on GAMM. In Canada, the trend is -0.10 μg/m^3/decade in Canada and the PM$_{2.5}$ concentration exhibits an east-high to west-low pattern. In the United States, the trend is -0.40 μg/m^3/decade, and PM$_{2.5}$ concentration decreases significantly after 1992, with a trend of -1.39 μg/m^3/decade. The high PM$_{2.5}$ concentration areas are in the east and west and the low are in the central and northern regions. In Europe, the trend is -1.55 μg/m^3/decade. High concentration areas are distributed in eastern Europe, while the low is in northern and western Europe. In China, the trend is 2.09 μg/m^3/decade. High concentration areas are distributed in northern China and the low are distributed in southern China and Northern Tianshan Mountains. The trend is 2.65μg/m^3/decade from 1959 to 2011 and -22.23 μg/m^3/decade from 2012 to 2022. In India, the trend is 0.92 μg/m^3/decade. The concentration exhibits a north-high to south-low pattern, with high concentration areas distributed in northern India, such as Ganges Plain and Thar Desert and the low in Deccan Plateau. The trend is 1.41 μg/m^3/decade from 1959 to 2013 and -23.36 μg/m^3/decade from 2014 to 2012. The variation of PM$_{2.5}$ concentration is inseparable with the implementation of pollution control laws and regulations, the energy structure, industrialization, population and vegetation coverage.

7 Data Availability

Daily PM$_{2.5}$ concentration data in the Northern Hemisphere from 1959 to 2022 are available at https://cstr.cn/18406.11.Atmos.tpdc.301127 (Hao et al., 2024).

All site-scale PM$_{2.5}$ data files are in "PM25-Daily_1959_2022. zip". The file name includes a region name and a site number. For example, the file name, 'China_1001. txt', means that the site is in China, and the site number is 1001, which describes the daily PM$_{2.5}$ concentration at a single site and can be directly opened using a text program (such as Notepad), separated by commas. The data includes four variables: Date, PM25(μg/m3), Longitude(degree_east), and Latitude(degree_north). Date is UTC time, PM25(μg/m3) is the daily PM$_{2.5}$ concentration (unit: μg/m^3), Longitude range is [-180 °E, 180 °E] and Latitude range is [0 °N, 90 °N].

Competing Interests

The contact author has declared that none of the authors has any competing interests.

Acknowledgments

This work was supported by the National Key Research & Development Program of China (2022YFF0801302) and the National Natural Science Foundation of China (41930970). The hourly visibility data are available at from https://www.ncei.noaa.gov/products/land-based-station/integrated-surface-database. The hourly $PM_{2.5}$ data for the United States are available at https://www.epa.gov/aqs. The hourly $PM_{2.5}$ data for Canada are available at https://www.canada.ca. The hourly $PM_{2.5}$ data for Europe available at https://european-union.europa.eu. The hourly $PM_{2.5}$ data for China are available at https://www.cnemc.cn. The hourly $PM_{2.5}$ data for India are available at https://app.cpcbccr.com. The hourly $PM_{2.5}$ concentration data of other regions are from openAQ, available at https://openaq.org. The daily $PM_{2.5}$ concentration of long-term gap-free high-resolution air pollutants (LGHAP) concentration dataset over global land, with a 1 km grid resolution, is available at https://zenodo.org/communities/ecnu_lghap.

References

Albrecht, B. A.: Aerosols, cloud microphysics, and fractional cloudiness, Science, 245, 1227-1230, https://doi.org/10.1126/science.245.4923.1227, 1989.

Ali, M. A., Bilal, M., Wang, Y., Nichol, J. E., Mhawish, A., Qiu, Z., de Leeuw, G., Zhang, Y., Zhan, Y., Liao, K., Almazroui, M., Dambul, R., Shahid, S., and Islam, M. N.: Accuracy assessment of CAMS and MERRA-2 reanalysis PM2.5 and PM10 concentrations over China, Atmos. Environ., 288, 119297, https://doi.org/10.1016/j.atmosenv.2022.119297, 2022.

Bai, K., Li, K., Shao, L., Li, X., Liu, C., Li, Z., Ma, M., Han, D., Sun, Y., Zheng, Z., Li, R., Chang, N. B., and Guo, J.: LGHAP v2: a global gap-free aerosol optical depth and PM2.5 concentration dataset since 2000 derived via big Earth data analytics, Earth Syst. Sci. Data, 16, 2425-2448, https://doi.org/10.5194/essd-16-2425-2024, 2024.

Beckerman, B. S., Jerrett, M., Serre, M., Martin, R. V., Lee, S.-J., Van Donkelaar, A., Ross, Z., Su, J., and Burnett, R. T.: A hybrid approach to estimating national scale spatiotemporal variability of PM2. 5 in the contiguous United States, Environ. Sci. Technol., 47, 7233-7241, https://doi.org/10.1021/es400039u, 2013.

Bergstrom, R. W., Pilewskie, P., Russell, P. B., Redemann, J., Bond, T. C., Quinn, P. K., and Sierau, B.: Spectral absorption properties of atmospheric aerosols, Atmos. Chem. Phys., 7, 5937-5943, https://doi.org/10.5194/acp-7-5937-2007, 2007.

Boers, R., van Weele, M., van Meijgaard, E., Savenije, M., Siebesma, A. P., Bosveld, F., and Stammes, P.: Observations and projections of visibility and aerosol optical thickness (1956-2100) in the Netherlands: impacts of time-varying aerosol composition and hygroscopicity, Environ. Res. Lett., 10, https://doi.org/10.1088/1748-9326/10/1/015003, 2015.

Boys, B., Martin, R., Van Donkelaar, A., MacDonell, R., Hsu, N., Cooper, M., Yantosca, R., Lu, Z., Streets, D., and Zhang, Q.: Fifteen-year global time series of satellite-derived fine particulate matter, Environ. Sci. Technol., 48, 11109-11118, https://doi.org/10.1021/es502113p, 2014.

Browne, M. W.: Cross-validation methods, J. Math. Psychol., 44, 108-132, https://doi.org/10.1006/jmps.1999.1279, 2000.

Buchard, V., da Silva, A. M., Colarco, P. R., Darmenov, A., Randles, C. A., Govindaraju, R., Torres, O., Campbell, J., and Spurr, R.: Using the OMI aerosol index and absorption aerosol optical depth to evaluate the NASA MERRA Aerosol Reanalysis, Atmos. Chem. Phys., 15, 5743-5760, https://doi.org/10.5194/acp-15-5743-2015, 2015.

Buchard, V., da Silva, A. M., Randles, C. A., Colarco, P., Ferrare, R., Hair, J., Hostetler, C., Tackett, J., and Winker, D.: Evaluation of the surface PM2.5 in Version 1 of the NASA MERRA Aerosol Reanalysis over the United States, Atmos. Environ., 125, 100-111, https://doi.org/10.1016/j.atmosenv.2015.11.004, 2016.

Buchard, V., Randles, C. A., da Silva, A. M., Darmenov, A., Colarco, P. R., Govindaraju, R., Ferrare, R., Hair, J., Beyersdorf, A. J., Ziemba, L. D., and Yu, H.: The MERRA-2 Aerosol Reanalysis, 1980 Onward. Part II: Evaluation and Case Studies, J. Climate, 30, 6851-6872, https://doi.org/10.1175/JCLI-D-16-0613.1, 2017.

Chafe, Z. A., Brauer, M., Klimont, Z., Van Dingenen, R., Mehta, S., Rao, S., Riahi, K., Dentener, F., and Smith, K. R.: Household Cooking with Solid Fuels Contributes to Ambient PM2.5 Air Pollution and the Burden of Disease, Environ. Health Persp., 122, 1314-1320, https://doi.org/10.1289/ehp.1206340, 2014.

Chang, K.-L., Petropavlovskikh, I., Cooper, O. R., Schultz, M. G., and Wang, T.: Regional trend analysis of surface ozone observations from monitoring networks in eastern North America, Europe and East Asia, Elementa: Science of the Anthropocene, 5, https://doi.org/10.1525/elementa.243, 2017.

Che, H., Xia, X., Zhu, J., Hong, W., and Shi, G.: Aerosol optical properties under the condition of heavy haze over an urban site of Beijing, China, Environ. Sci. Pollut. R., 22, 1043-1053, https://doi.org/10.1007/s11356-014-3415-5, 2014.

Chen, A., Zhao, C., and Fan, T.: Spatio-temporal distribution of aerosol direct radiative forcing over mid-latitude regions in north hemisphere estimated from satellite observations, Atmos. Res., 266, 105938, https://doi.org/10.1016/j.atmosres.2021.105938, 2022.

Chen, Z., Chen, D., Zhao, C., Kwan, M.-p., Cai, J., Zhuang, Y., Zhao, B., Wang, X., Chen, B., Yang, J., Li, R., He, B., Gao, B., Wang, K., and Xu, B.: Influence of meteorological conditions on PM2.5 concentrations across China: A review of methodology and mechanism, Environ. Int., 139, https://doi.org/10.1016/j.envint.2020.105558, 2020.

Chow, J. C., Doraiswamy, P., Watson, J. G., Chen, L. W. A., Ho, S. S. H., and Sodeman, D. A.: Advances in Integrated and Continuous Measurements for Particle Mass and Chemical Composition, Japca J. Air Waste Ma., 58, 141-163, https://doi.org/10.3155/1047-3289.58.2.141, 2008.

Cohen, A. J., Brauer, M., Burnett, R., Anderson, H. R., Frostad, J., Estep, K., Balakrishnan, K., Brunekreef, B., Dandona, L., Dandona, R., Feigin, V., Freedman, G., Hubbell, B., Jobling, A., Kan, H., Knibbs, L., Liu, Y., Martin, R., Morawska, L., Pope, C. A., III, Shin, H., Straif, K., Shaddick, G., Thomas, M., van Dingenen, R., van Donkelaar, A., Vos, T., Murray, C. J. L., and Forouzanfar, M. H.: Estimates and 25-year trends of the global burden of disease attributable to ambient air pollution: an analysis of data from the Global Burden of Diseases Study 2015, Lancet, 389, 1907-1918, https://doi.org/10.1016/s0140-6736(17)30505-6, 2017.

Dabek-Zlotorzynska, E., Dann, T. F., Martinelango, P. K., Celo, V., Brook, J. R., Mathieu, D., Ding, L., and Austin, C. C.: Canadian National Air Pollution Surveillance (NAPS) PM2.5 speciation program: Methodology and PM2.5 chemical composition for the years 2003-2008, Atmos. Environ., 45, 673-686, https://doi.org/10.1016/j.atmosenv.2010.10.024, 2011.

Davies, J.: CEPA—The Canadian. Environmental Protection Act, JAPCA, 38, 1111-1113, https://doi.org/10.1080/08940630.1988.10466452, 1988.

Demerjian, K. L.: A review of national monitoring networks in North America, Atmos. Environ., 34, 1861-1884, https://doi.org/10.1016/S1352-2310(99)00452-5, 2000.

Fan, H., Zhao, C., Yang, Y., and Yang, X.: Spatio-Temporal Variations of the $PM_{2.5}/PM_{10}$ Ratios and Its Application to Air Pollution Type Classification in China, Front. Environ. Sci., 9, https://doi.org/10.3389/fenvs.2021.692440, 2021.

Friedman, J. H.: Greedy function approximation: A gradient boosting machine, Ann. Stat., 29, 1189-1232, https://doi.org/10.1214/aos/1013203451, 2001.

Ganguly, T., Selvaraj, K. L., and Guttikunda, S. K.: National Clean Air Programme (NCAP) for Indian cities: Review and outlook of clean air action plans, Atmospheric Environment X, 8, 100096, https://doi.org/10.1016/j.aeaoa.2020.100096, 2020.

Gelaro, R., McCarty, W., Suárez, M. J., Todling, R., Molod, A., Takacs, L., Randles, C. A., Darmenov, A., Bosilovich, M. G., Reichle, R., Wargan, K., Coy, L., Cullather, R., Draper, C., Akella, S., Buchard, V., Conaty, A., da Silva, A. M., Gu, W., Kim, G.-K., Koster, R., Lucchesi, R., Merkova, D., Nielsen, J. E., Partyka, G., Pawson, S., Putman, W., Rienecker, M., Schubert, S. D., Sienkiewicz, M., and Zhao, B.: The Modern-Era Retrospective Analysis for Research and Applications, Version 2 (MERRA-2), J. Climate, 30, 5419-5454, https://doi.org/10.1175/JCLI-D-16-0758.1, 2017.

Goff, J. A.: Saturation pressure of water on the new Kelvin temperature scale, Transactions of the American Society of Heating and Ventilating Engineers, 63, 347-354, 1957.

Granier, C., Bessagnet, B., Bond, T., D'Angiola, A., Denier van der Gon, H., Frost, G. J., Heil, A., Kaiser, J. W., Kinne, S., and Klimont, Z.: Evolution of anthropogenic and biomass burning emissions of air pollutants at global and regional scales during the 1980–2010 period, Climatic Change, 109, 163-190, https://doi.org/10.1007/s10584-011-0154-1, 2011.

Green, D. and Fuller, G. W.: The implications of tapered element oscillating microbalance (TEOM) software configuration on particulate matter measurements in the UK and Europe, Atmos. Environ., 40, 5608-5616, https://doi.org/10.1016/j.atmosenv.2006.04.052, 2006.

Gui, K., Che, H., Zeng, Z., Wang, Y., Zhai, S., Wang, Z., Luo, M., Zhang, L., Liao, T., and Zhao, H.: Construction of a virtual PM2. 5 observation network in China based on high-density surface meteorological observations using the Extreme Gradient Boosting model, Environ. Int., 141, 105801, https://doi.org/10.1016/j.envint.2020.105801, 2020.

Guo, S., Hu, M., Zamora, M. L., Peng, J., Shang, D., Zheng, J., Du, Z., Wu, Z., Shao, M., Zeng, L., Molina, M. J., and Zhang, R.: Elucidating severe urban haze formation in China, P. Natl. A. Sci., 111, 17373-17378, https://doi.org/10.1073/pnas.1419604111, 2014.

Hall, E. and Gilliam, J.: Reference and Equivalent Methods Used to Measure National Ambient Air Quality Standards (NAAQS) Criteria Air Pollutants - Volume I, https://doi.org/10.13140/RG.2.1.3471.8329, 2016.

Hammer, M. S., van Donkelaar, A., Li, C., Lyapustin, A., Sayer, A. M., Hsu, N. C., Levy, R. C., Garay, M. J., Kalashnikova, O. V., and Kahn, R. A.: Global estimates and long-term trends of fine particulate matter concentrations (1998–2018), Environ. Sci. Technol., 54, 7879-7890, https://doi.org/10.1021/acs.est.0c01764, 2020.

Hao, H., Wang, K., Wu, G., Liu, J., and Li, J.: PM2.5 concentrations based on near-surface visibility at 4011 sites in the Northern Hemisphere from 1959 to 2022, National Tibetan Plateau Data Center [dataset], https://doi.org/10.11888/Atmos.tpdc.301127, 2024.

Hastie, T. and Tibshirani, R.: Generalized Additive Models: Some Applications, J. Am. Stat. Assoc., 82, 371-386, https://doi.org/10.1080/01621459.1987.10478440, 1987.

He, Q., Gao, K., Zhang, L., Song, Y., and Zhang, M.: Satellite-derived 1-km estimates and long-term trends of PM2. 5 concentrations in China from 2000 to 2018, Environ. Int., 156, 106726, https://doi.org/10.1016/j.envint.2021.106726, 2021.

Hsu, N., Lee, J., Sayer, A., Carletta, N., Chen, S. H., Tucker, C., Holben, B., and Tsay, S. C.: Retrieving near‑global aerosol loading over land and ocean from AVHRR, J. Geophys. Res-Atmos., 122, 9968-9989, https://doi.org/10.1002/2017JD026932, 2017.

Huang, W., Tan, J., Kan, H., Zhao, N., Song, W., Song, G., Chen, G., Jiang, L., Jiang, C., and Chen, R.: Visibility, air quality and daily mortality in Shanghai, China, Sci. Total Environ., 407, 3295-3300, https://doi.org/10.1016/j.scitotenv.2009.02.019, 2009.

Husar, R. B., Husar, J. D., and Martin, L.: Distribution of continental surface aerosol extinction based on visual range data, Atmos. Environ., 34, 5067-5078, https://doi.org/10.1016/s1352-2310(00)00324-1, 2000.

Inness, A., Ades, M., Agustí-Panareda, A., Barré, J., Benedictow, A., Blechschmidt, A.-M., Dominguez, J. J., Engelen, R., Eskes, H., and Flemming, J.: The CAMS reanalysis of atmospheric composition, Atmos. Chem. Phys., 19, 3515-3556, https://doi.org/10.5194/acp-19-3515-2019, 2019.

Jin, C., Wang, Y., Li, T., and Yuan, Q.: Global validation and hybrid calibration of CAMS and MERRA-2 PM2.5 reanalysis products based on OpenAQ platform, Atmos. Environ., 274, 118972, https://doi.org/10.1016/j.atmosenv.2022.118972, 2022.

Kammann, E. E. and Wand, M. P.: Geoadditive Models, J. R. Stat. Soc. C-appl., 52, 1-18, https://doi.org/10.1111/1467-9876.00385, 2003.

Kendall, M. G.: Rank correlation methods, 1948.

Kim, K.-H., Kabir, E., and Kabir, S.: A review on the human health impact of airborne particulate matter, Environ. Int., 74, 136-143, https://doi.org/10.1016/j.envint.2014.10.005, 2015.

Kuklinska, K., Wolska, L., and Namiesnik, J.: Air quality policy in the US and the EU–a review, Atmos. Pollut. Res., 6, 129-137, https://doi.org/10.5094/APR.2015.015, 2015.

Lelieveld, J., Evans, J. S., Fnais, M., Giannadaki, D., and Pozzer, A.: The contribution of outdoor air pollution sources to premature mortality on a global scale, Nature, 525, 367-+, https://doi.org/10.1038/nature15371, 2015.

Li, C., Martin, R. V., Boys, B. L., van Donkelaar, A., and Ruzzante, S.: Evaluation and application of multi-decadal visibility data for trend analysis of atmospheric haze, Atmos. Chem. Phys., 16, 2435-2457, https://doi.org/10.5194/acp-16-2435-2016, 2016.

Li, C., Martin, R. V., van Donkelaar, A., Boys, B. L., Hammer, M. S., Xu, J.-W, Marais, E. A., Reff, A., Strum, M., and Ridley, D. A.: Trends in chemical composition of global and regional population-weighted fine particulate matter estimated for 25 years, Environ. Sci. Technol., 51, 11185-11195, https://doi.org/10.1021/acs.est.7b02530, 2017.

Li, J., Han, X., Jin, M., Zhang, X., and Wang, S.: Globally analysing spatiotemporal trends of anthropogenic PM2. 5 concentration and population's PM2. 5 exposure from 1998 to 2016, Environ. Int., 128, 46-62, https://doi.org/10.1016/j.envint.2019.04.026, 2019.

Li, J., Garshick, E., Hart, J. E., Li, L., Shi, L., Al-Hemoud, A., Huang, S., and Koutrakis, P.: Estimation of ambient PM2.5 in Iraq and Kuwait from 2001 to 2018 using machine learning and remote sensing, Environ. Int., 151, https://doi.org/10.1016/j.envint.2021.106445, 2021.

Li, J., Carlson, B. E., Yung, Y. L., Lv, D., Hansen, J., Penner, J. E., Liao, H., Ramaswamy, V., Kahn, R. A., Zhang, P., Dubovik, O., Ding, A., Lacis, A. A., Zhang, L., and Dong, Y.: Scattering and absorbing aerosols in the climate system, Nat. Rev. Earth. Environ., 3, 363-379, https://doi.org/10.1038/s43017-

1048   022-00296-7, 2022.

1049   Li, S., Chen, L., Huang, G., Lin, J., Yan, Y., Ni, R., Huo, Y., Wang, J., Liu, M., and Weng, H.: Retrieval
1050   of surface PM2. 5 mass concentrations over North China using visibility measurements and GEOS-Chem
1051   simulations, Atmos. Environ., 222, 117121, https://doi.org/10.1016/j.atmosenv.2019.117121, 2020.

1052   Liao, H., Chang, W., and Yang, Y.: Climatic Effects of Air Pollutants over China: A Review, Adv. Atmos.
1053   Sci., 32, 115-139, https://doi.org/10.1007/s00376-014-0013-x, 2015.

1054   Lim, C.-H., Ryu, J., Choi, Y., Jeon, S. W., and Lee, W.-K.: Understanding global PM2. 5 concentrations
1055   and their drivers in recent decades (1998–2016), Environ. Int., 144, 106011,
1056   https://doi.org/10.1016/j.envint.2020.106011, 2020.

1057   Liu, M., Bi, J., and Ma, Z.: Visibility-based PM2. 5 concentrations in China: 1957–1964 and 1973–2014,
1058   Environ. Sci. Technol., 51, 13161-13169, https://doi.org/10.1021/acs.est.7b03468, 2017.

1059   Liu, M., Huang, X., Song, Y., Tang, J., Cao, J., Zhang, X., Zhang, Q., Wang, S., Xu, T., Kang, L., Cai,
1060   X., Zhang, H., Yang, F., Wang, H., Yu, J. Z., Lau, A. K. H., He, L., Huang, X., Duan, L., Ding, A., Xue,
1061   L., Gao, J., Liu, B., and Zhu, T.: Ammonia emission control in China would mitigate haze pollution and
1062   nitrogen deposition, but worsen acid rain, P. Natl. A. Sci., 116, 7760-7765,
1063   https://doi.org/10.1073/pnas.1814880116, 2019.

1064   Ma, Z., Hu, X., Sayer, A. M., Levy, R., Zhang, Q., Xue, Y., Tong, S., Bi, J., Huang, L., and Liu, Y.:
1065   Satellite-based spatiotemporal trends in PM2. 5 concentrations: China, 2004–2013, Environ. Health
1066   Persp., 124, 184-192, https://doi.org/10.1289/ehp.1409481, 2016.

1067   Mandal, S., Madhipatla, K. K., Guttikunda, S., Kloog, I., Prabhakaran, D., Schwartz, J. D., and Team, G.
1068   H. I.: Ensemble averaging based assessment of spatiotemporal variations in ambient PM2. 5
1069   concentrations over Delhi, India, during 2010–2016, Atmos. Environ., 224, 117309,
1070   https://doi.org/10.1016/j.atmosenv.2020.117309, 2020.

1071   Mann, H. B.: Nonparametric Tests Against Trend, Econometrica, 13, 245-259,
1072   https://doi.org/10.2307/1907187, 1945.

1073   Meng, X., Hand, J. L., Schichtel, B. A., and Liu, Y.: Space-time trends of PM2. 5 constituents in the
1074   conterminous United States estimated by a machine learning approach, 2005–2015, Environ. Int., 121,
1075   1137-1147, https://doi.org/10.1016/j.envint.2018.10.029, 2018.

1076   Miao, Y. and Liu, S.: Linkages between aerosol pollution and planetary boundary layer structure in China,
1077   Sci. Total Environ., 650, 288-296, https://doi.org/10.1016/j.scitotenv.2018.09.032, 2019.

1078   Molnár, A., Mészáros, E., Imre, K., and Rüll, A.: Trends in visibility over Hungary between 1996 and
1079   2002, Atmos. Environ., 42, 2621-2629, https://doi.org/10.1016/j.atmosenv.2007.05.012, 2008.

1080   Nagaraja Rao, C., Stowe, L., and McClain, E.: Remote sensing of aerosols over the oceans using AVHRR
1081   data Theory, practice and applications, Int. J. Remote Sens., 10, 743-749,
1082   https://doi.org/10.1080/01431168908903915, 1989.

1083   NOAA, DOD, FAA, and USN: Automated Surface Observing System (ASOS) User's Guide, 1998.

1084   Pant, P., Lal, R. M., Guttikunda, S. K., Russell, A. G., Nagpure, A. S., Ramaswami, A., and Peltier, R. E.:
1085   Monitoring particulate matter in India: recent trends and future outlook, Air. Qual. Tmos. Hlth., 12, 45-
1086   58, https://doi.org/10.1007/s11869-018-0629-6, 2019.

1087   Park, A., Guillas, S., and Petropavlovskikh, I.: Trends in stratospheric ozone profiles using functional
1088   mixed models, Atmos. Chem. Phys., 13, 11473-11501, https://doi.org/10.5194/acp-13-11473-2013, 2013.

1089   Polansky, L. and Robbins, M. M.: Generalized additive mixed models for disentangling long-term trends,
1090   local anomalies, and seasonality in fruit tree phenology, Ecol. Evol., 3, 3141-3151,
1091   https://doi.org/10.1002/ece3.707, 2013.

Pui, D. Y. H., Chen, S.-C., and Zuo, Z.: PM2.5 in China: Measurements, sources, visibility and health effects, and mitigation, Particuology, 13, 1-26, https://doi.org/10.1016/j.partic.2013.11.001, 2014.

Qi, G., Wei, W., Wang, Z., Wang, Z., and Wei, L.: The spatial-temporal evolution mechanism of PM2. 5 concentration based on China's climate zoning, J. Environ. Manage., 325, 116671, https://doi.org/10.1016/j.jenvman.2022.116671, 2023.

Ramanathan, V., Crutzen, P. J., Kiehl, J., and Rosenfeld, D.: Aerosols, climate, and the hydrological cycle, Science, 294, 2119-2124, https://doi.org/10.1126/science.1064034, 2001.

Ravindra, K., Rattan, P., Mor, S., and Aggarwal, A. N.: Generalized additive models: Building evidence of air pollution, climate change and human health, Environ. Int., 132, 104987, https://doi.org/10.1016/j.envint.2019.104987, 2019.

Ravindra, K., Vakacherla, S., Singh, T., Upadhya, A. R., Rattan, P., and Mor, S.: Long-term trend of PM2.5 over five Indian megacities using a new statistical approach, Stoch. Env. Res. Risk A., 38, 715-725, https://doi.org/10.1007/s00477-023-02595-x, 2024.

Samset, B. H., Lund, M. T., Bollasina, M., Myhre, G., and Wilcox, L.: Emerging Asian aerosol patterns, Nat. Geosci., 12, 582-584, https://doi.org/10.1038/s41561-019-0424-5, 2019.

Sen, P. K.: Estimates of the Regression Coefficient Based on Kendall's Tau, J. Am. Stat. Assoc., 63, 1379-1389, https://doi.org/10.1080/01621459.1968.10480934, 1968.

Shen, Z., Cao, J., Zhang, L., Zhang, Q., Huang, R.-J., Liu, S., Zhao, Z., Zhu, C., Lei, Y., and Xu, H.: Retrieving historical ambient PM2. 5 concentrations using existing visibility measurements in Xi'an, Northwest China, Atmos. Environ., 126, 15-20, https://doi.org/10.1016/j.atmosenv.2015.11.040, 2016.

Shi, Y., Matsunaga, T., Yamaguchi, Y., Li, Z., Gu, X., and Chen, X.: Long-term trends and spatial patterns of satellite-retrieved PM2. 5 concentrations in South and Southeast Asia from 1999 to 2014, Sci. Total Environ., 615, 177-186, https://doi.org/10.1016/j.scitotenv.2017.09.241, 2018.

Singh, A., Avis, W. R., and Pope, F. D.: Visibility as a proxy for air quality in East Africa, Environ. Res. Lett., 15, 084002, https://doi.org/10.1088/1748-9326/ab8b12, 2020.

Singh, V., Singh, S., and Biswal, A.: Exceedances and trends of particulate matter (PM2.5) in five Indian megacities, Sci. Total Environ., 750, 141461, https://doi.org/10.1016/j.scitotenv.2020.141461, 2021.

Smith, A., Lott, N., and Vose, R.: The Integrated Surface Database: Recent Developments and Partnerships, B. Am. Meteorol. Soc., 92, 704-708, https://doi.org/10.1175/2011BAMS3015.1, 2011.

Su, L., Gao, C., Ren, X., Zhang, F., Cao, S., Zhang, S., Chen, T., Liu, M., Ni, B., and Liu, M.: Understanding the spatial representativeness of air quality monitoring network and its application to PM2.5 in the mainland China, Geosci. Front., 13, 101370, https://doi.org/10.1016/j.gsf.2022.101370, 2022.

Sun, E., Xu, X., Che, H., Tang, Z., Gui, K., An, L., Lu, C., and Shi, G.: Variation in MERRA-2 aerosol optical depth and absorption aerosol optical depth over China from 1980 to 2017, J. Atmos. Sol-Terr. Phy., 186, 8-19, https://doi.org/10.1016/j.jastp.2019.01.019, 2019.

Tan, S., Wang, Y., Yuan, Q., Zheng, L., Li, T., Shen, H., and Zhang, L.: Reconstructing global PM2.5 monitoring dataset from OpenAQ using a two-step spatio-temporal model based on SES-IDW and LSTM, Environ. Res. Lett., 17, 034014, https://doi.org/10.1088/1748-9326/ac52c9, 2022.

Theil, H.: A Rank-Invariant Method of Linear and Polynomial Regression Analysis, in: Henri Theil's Contributions to Economics and Econometrics: Econometric Theory and Methodology, edited by: Raj, B., and Koerts, J., Springer Netherlands, Dordrecht, 345-381, https://doi.org/10.1007/978-94-011-2546-8_20, 1992.

Van Donkelaar, A., Martin, R. V., and Park, R. J.: Estimating ground-level PM2. 5 using aerosol optical

depth determined from satellite remote sensing, J. Geophys. Res., 111, https://doi.org/10.1029/2005JD006996, 2006.

Van Donkelaar, A., Martin, R. V., Brauer, M., and Boys, B. L.: Use of satellite observations for long-term exposure assessment of global concentrations of fine particulate matter, Environ. Health Persp., 123, 135-143, https://doi.org/10.1289/ehp.1408646, 2015.

Van Donkelaar, A., Martin, R. V., Brauer, M., Kahn, R., Levy, R., Verduzco, C., and Villeneuve, P. J.: Global estimates of ambient fine particulate matter concentrations from satellite-based aerosol optical depth: development and application, Environ. Health Persp., 118, 847-855, https://doi.org/10.1289/ehp.0901623, 2010.

Van Donkelaar, A., Martin, R. V., Brauer, M., Hsu, N. C., Kahn, R. A., Levy, R. C., Lyapustin, A., Sayer, A. M., and Winker, D. M.: Global estimates of fine particulate matter using a combined geophysical-statistical method with information from satellites, models, and monitors, Environ. Sci. Technol., 50, 3762-3772, https://doi.org/10.1021/acs.est.5b05833, 2016.

van Donkelaar, A., Hammer, M. S., Bindle, L., Brauer, M., Brook, J. R., Garay, M. J., Hsu, N. C., Kalashnikova, O. V., Kahn, R. A., Lee, C., Levy, R. C., Lyapustin, A., Sayer, A. M., and Martin, R. V.: Monthly Global Estimates of Fine Particulate Matter and Their Uncertainty, Environ. Sci. Technol., 55, 15287-15300, https://doi.org/10.1021/acs.est.1c05309, 2021.

Verbeke, G. and Lesaffre, E.: A Linear Mixed-Effects Model with Heterogeneity in the Random-Effects Population, J. Am. Stat. Assoc., 91, 217-221, https://doi.org/10.1080/01621459.1996.10476679, 1996.

Viana, M., Kuhlbusch, T. A. J., Querol, X., Alastuey, A., Harrison, R. M., Hopke, P. K., Winiwarter, W., Vallius, A., Szidat, S., Prevot, A. S. H., Hueglin, C., Bloemen, H., Wahlin, P., Vecchi, R., Miranda, A. I., Kasper-Giebl, A., Maenhaut, W., and Hitzenberger, R.: Source apportionment of particulate matter in Europe: A review of methods and results, J. Aerosol Sci., 39, 827-849, https://doi.org/10.1016/j.jaerosci.2008.05.007, 2008.

Wang, K., Dickinson, R. E., and Liang, S.: Clear Sky Visibility Has Decreased over Land Globally from 1973 to 2007, Science, 323, 1468-1470, https://doi.org/10.1126/science.1167549, 2009.

Wang, K. C., Dickinson, R. E., Su, L., and Trenberth, K. E.: Contrasting trends of mass and optical properties of aerosols over the Northern Hemisphere from 1992 to 2011, Atmos. Chem. Phys., 12, 9387-9398, https://doi.org/10.5194/acp-12-9387-2012, 2012.

Wang, Q., Kwan, M.-P., Zhou, K., Fan, J., Wang, Y., and Zhan, D.: The impacts of urbanization on fine particulate matter (PM2. 5) concentrations: Empirical evidence from 135 countries worldwide, Environ. Pollut., 247, 989-998, https://doi.org/10.1016/j.envpol.2019.01.086, 2019.

Wang, Z., Li, J., Wang, Z., Yang, W., Tang, X., Ge, B., Yan, P., Zhu, L., Chen, X., Chen, H., Wand, W., Li, J., Liu, B., Wang, X., Wand, W., Zhao, Y., Lu, N., and Su, D.: Modeling study of regional severe hazes over mid-eastern China in January 2013 and its implications on pollution prevention and control, Sci. China Earth Sci., 57, 3-13, https://doi.org/10.1007/s11430-013-4793-0, 2014.

Wei, J., Li, Z., Peng, Y., and Sun, L.: MODIS Collection 6.1 aerosol optical depth products over land and ocean: validation and comparison, Atmos. Environ., 201, 428-440, https://doi.org/10.1016/j.atmosenv.2018.12.004, 2019a.

Wei, J., Huang, W., Li, Z., Xue, W., Peng, Y., Sun, L., and Cribb, M.: Estimating 1-km-resolution PM2.5 concentrations across China using the space-time random forest approach, Remote Sens. Environ., 231, https://doi.org/10.1016/j.rse.2019.111221, 2019b.

Wei, J., Li, Z., Lyapustin, A., Sun, L., Peng, Y., Xue, W., Su, T., and Cribb, M.: Reconstructing 1-km-resolution high-quality PM2. 5 data records from 2000 to 2018 in China: spatiotemporal variations and

policy implications, Remote Sens. Environ., 252, 112136, https://doi.org/10.1016/j.rse.2020.112136, 2021.

Wei, J., Li, Z., Cribb, M., Huang, W., Xue, W., Sun, L., Guo, J., Peng, Y., Li, J., and Lyapustin, A.: Improved 1 km resolution PM 2.5 estimates across China using enhanced space–time extremely randomized trees, Atmos. Chem. Phys., 20, 3273-3289, https://doi.org/10.5194/acp-20-3273-2020, 2020.

Wood, S. N., Pya, N., and Säfken, B.: Smoothing Parameter and Model Selection for General Smooth Models, J. Am. Stat. Assoc., 111, 1548-1563, https://doi.org/10.1080/01621459.2016.1180986, 2016.

Wu, J., Zheng, H., Zhe, F., Xie, W., and Song, J.: Study on the relationship between urbanization and fine particulate matter (PM2. 5) concentration and its implication in China, J. Cleaner Prod., 182, 872-882, https://doi.org/10.1016/j.jclepro.2018.02.060, 2018.

Wu, W. and Zhang, Y.: Effects of particulate matter (PM2.5) and associated acidity on ecosystem functioning: response of leaf litter breakdown, Environ. Sci. Pollut. R., 25, 30720-30727, https://doi.org/10.1007/s11356-018-2922-1, 2018.

Xue, T., Zheng, Y., Tong, D., Zheng, B., Li, X., Zhu, T., and Zhang, Q.: Spatiotemporal continuous estimates of PM2. 5 concentrations in China, 2000–2016: A machine learning method with inputs from satellites, chemical transport model, and ground observations, Environ. Int., 123, 345-357, https://doi.org/10.1016/j.envint.2018.11.075, 2019.

Yang, X., Zhao, C., Yang, Y., Yan, X., and Fan, H.: Statistical aerosol properties associated with fire events from 2002 to 2019 and a case analysis in 2019 over Australia, Atmos. Chem. Phys., 21, 3833-3853, https://doi.org/10.5194/acp-21-3833-2021, 2021.

Zeng, Z., Gui, K., Wang, Z., Luo, M., Geng, H., Ge, E., An, J., Song, X., Ning, G., and Zhai, S.: Estimating hourly surface PM2. 5 concentrations across China from high-density meteorological observations by machine learning, Atmos. Res., 254, 105516, https://doi.org/10.1016/j.atmosres.2021.105516, 2021.

Zhang, Q., Zheng, Y., Tong, D., Shao, M., Wang, S., Zhang, Y., Xu, X., Wang, J., He, H., Liu, W., Ding, Y., Lei, Y., Li, J., Wang, Z., Zhang, X., Wang, Y., Cheng, J., Liu, Y., Shi, Q., Yan, L., Geng, G., Hong, C., Li, M., Liu, F., Zheng, B., Cao, J., Ding, A., Gao, J., Fu, Q., Huo, J., Liu, B., Liu, Z., Yang, F., He, K., and Hao, J.: Drivers of improved PM$_{2.5}$ air quality in China from 2013 to 2017, P. Natl. A. Sci., 116, 24463-24469, https://doi.org/10.1073/pnas.1907956116, 2019.

Zhang, S., Wu, J., Fan, W., Yang, Q., and Zhao, D.: Review of aerosol optical depth retrieval using visibility data, Earth-Sci. Rev., 200, 102986, https://doi.org/10.1016/j.earscirev.2019.102986, 2020.

Zhang, Z., Wu, W., Wei, J., Song, Y., Yan, X., Zhu, L., and Wang, Q.: Aerosol optical depth retrieval from visibility in China during 1973-2014, Atmos. Environ., 171, 38-48, https://doi.org/10.1016/j.atmosenv.2017.09.004, 2017.

Zhao, B., Su, Y., He, S., Zhong, M., and Cui, G.: Evolution and comparative assessment of ambient air quality standards in China, J. Integr. Environ. Sci., 13, 85-102, https://doi.org/10.1080/1943815X.2016.1150301, 2016a.

Zhao, S., Yu, Y., Yin, D., He, J., Liu, N., Qu, J., and Xiao, J.: Annual and diurnal variations of gaseous and particulate pollutants in 31 provincial capital cities based on in situ air quality monitoring data from China National Environmental Monitoring Center, Environ. Int., 86, 92-106, https://doi.org/10.1016/j.envint.2015.11.003, 2016b.

Zhong, J., Zhang, X., Gui, K., Liao, J., Fei, Y., Jiang, L., Guo, L., Liu, L., Che, H., and Wang, Y.: Reconstructing 6-hourly PM 2.5 datasets from 1960 to 2020 in China, Earth Syst. Sci. Data, 14, 3197-3211, https://doi.org/10.5194/essd-14-3197-2022, 2022.

1224   Zhong, J., Zhang, X., Gui, K., Wang, Y., Che, H., Shen, X., Zhang, L., Zhang, Y., Sun, J., and Zhang, W.:

1225   Robust prediction of hourly PM2. 5 from meteorological data using LightGBM, Natl. Sci. Rev., 8,

1226   nwaa307, https://doi.org/10.1093/nsr/nwaa307, 2021.

1227